AD-A138 485 MEASUREMENTS OF DIRECT PATH AND FOLDED PATH OPTICAL SCINTILLATION USING A CORNER CUBE REFLECTORS(U) NAVAL POSTGRADUATE SCHOOL MONTEREY CA L M HENRY DEC 83 1/1

UNCLASSIFIED F/G 20/6 NL

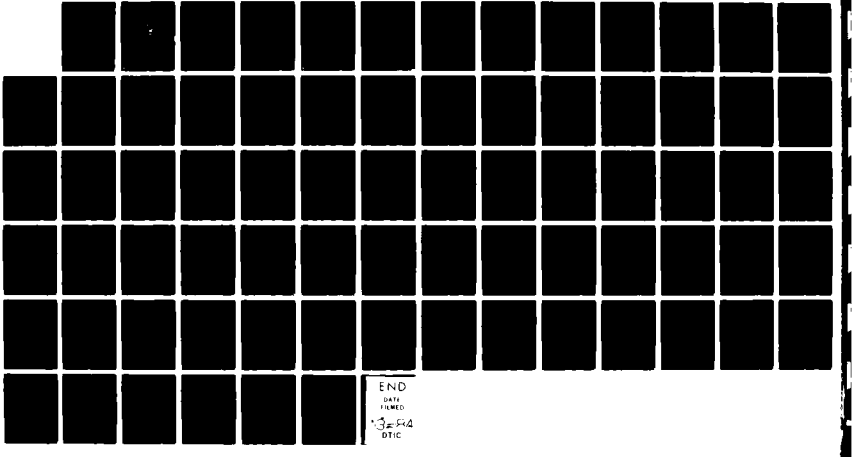

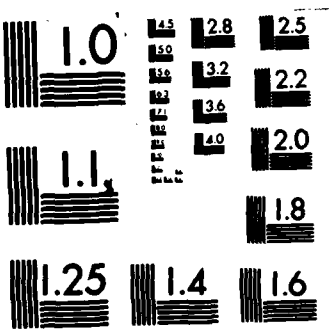

NAVAL POSTGRADUATE SCHOOL
Monterey, California

THESIS

MEASUREMENTS OF DIRECT PATH
AND FOLDED PATH OPTICAL SCINTILLATION
USING A CORNER CUBE REFLECTOR

by

Leon M. Henry
December 1983

Thesis Advisor: E. A. Milne

SECURITY CLASSIFICATION OF THIS PAGE (When Data Entered)

REPORT DOCUMENTATION PAGE		READ INSTRUCTIONS BEFORE COMPLETING FORM
1. REPORT NUMBER	2. GOVT ACCESSION NO. A138485	3. RECIPIENT'S CATALOG NUMBER
4. TITLE (and Subtitle) Measurements of Direct Path and Folded Path Optical Scintillation Using a Corner Cube Reflector		5. TYPE OF REPORT & PERIOD COVERED Master's Thesis; December 1983 6. PERFORMING ORG. REPORT NUMBER
7. AUTHOR(s) Leon M. Henry		8. CONTRACT OR GRANT NUMBER(s)
9. PERFORMING ORGANIZATION NAME AND ADDRESS Naval Postgraduate School Monterey, California 93943		10. PROGRAM ELEMENT, PROJECT, TASK AREA & WORK UNIT NUMBERS
11. CONTROLLING OFFICE NAME AND ADDRESS Naval Postgraduate School Monterey, California 93943		12. REPORT DATE December 1983 13. NUMBER OF PAGES 73
14. MONITORING AGENCY NAME & ADDRESS(if different from Controlling Office)		15. SECURITY CLASS. (of this report) Unclassified 15a. DECLASSIFICATION/DOWNGRADING SCHEDULE

16. DISTRIBUTION STATEMENT (of this Report)

Approved for public release; distribution unlimited.

17. DISTRIBUTION STATEMENT (of the abstract entered in Block 20, if different from Report)

18. SUPPLEMENTARY NOTES

19. KEY WORDS (Continue on reverse side if necessary and identify by block number)

Scintillation Path Weighting

20. ABSTRACT (Continue on reverse side if necessary and identify by block number)

A theoretical prediction of path weighting for optical scintillation strength was made by Dr. Avihu Ze'evi. As part of a continuing effort at NPS to verify the prediction, a sixty-one meter enclosed tunnel was constructed, allowing the position of a turbulence source to be varied. This experiment tested the Ze'evi hypothesis using a corner cube reflector. The results confirm patterns found in previous

DD FORM 1 JAN 73 1473 EDITION OF 1 NOV 65 IS OBSOLETE
S/N 0102-LF-014-6601

SECURITY CLASSIFICATION OF THIS PAGE (When Data Entered)

experiments, and the general form of the predicted path weighting. However, questions concerning the nature of the turbulence present in the tunnel do not allow strong conclusions to be formed.

A-1

Approved for public release; distribution unlimited

Measurements of Direct Path and Folded Path Optical Scintillation Using a Corner Cube Reflector

by

Leon M. Henry
Lieutenant, United States Navy
A.B., College of the Holy Cross, 1977

Submitted in partial fulfillment of the
requirements for the degree of

MASTER OF SCIENCE IN PHYSICS

from the

NAVAL POSTGRADUATE SCHOOL
December 1983

Author: Leon M. Henry

Approved by: Edmund A. Milne
Thesis Advisor

E. L. Crittenden, Jr.
Second Reader

Y.E. Strausser
Chairman, Department of Physics

J.N. Dyer
Dean of Science and Engineering

ABSTRACT

A theoretical prediction of path weighting for optical scintillation strength was made by Dr. Avihu Ze'evi. As part of a continuing effort at NPS to verify the prediction, a sixty-one meter enclosed tunnel was constructed, allowing the position of a turbulence source to be varied. This experiment tested the Ze'evi hypothesis using a corner cube reflector. The results confirm patterns found in previous experiments, and the general form of the predicted path weighting. However, questions concerning the nature of the turbulence present in the tunnel do not allow strong conclusions to be formed.

TABLE OF CONTENTS

ACKNOWLEDGEMENT

At this time we would like to express our appreciation to the many people who have offered generously of their time and experience. Without their generosity, the completion of this project would have been infinitely more difficult.

The experience and technical assistance of Mr. Robert Moeller, Mr. Robert Smith, Mr. Don Spiel, and Mr. Tom Maris proved crucial in the maintenance and repair of optical and electrical equipments.

The advice and support of Mr. Michael Drong and Mr. Kurt Stevens was always welcome. The insight offered by Professor E.C. Crittenden and Dr. Don Walters, was invaluable in the analysis of the work.

Finally, our thanks to Professor E.A. Milne for his patient, ever present guidance and direction.

I. INTRODUCTION

A. GENERAL

The effects of a non-uniform atmosphere on the propagation of optical radiation are many. The most familiar in everyday experience is seen in the twinkling of the stars, and is known as scintillation. Scintillation results from the random fluctuations of the index of refraction of the atmosphere causing the electromagnetic wave to be bent, and to suffer interference. These interference effects are recognized by an observer as changes in the irradiance, or intensity of the incident radiation.

B. THEORY

Since the refractive index fluctuations are random, statistical methods are used to describe the resulting behavior. One generally accepted form is derived by Tatarski [Ref. 1], and uses the normalized log-amplitude variance,

$$\sigma_A^2 = A\, K^{7/6}\, C_n^2\, L^{11/6} \qquad (1.1)$$

where $K = 2\pi/\lambda$

λ = the wavelength

C_n^2 = the refractive index structure constant

L = path distance, source to receiver

A = numeric constant, .3 for plane waves, .124 for spherical waves.

Under appropriate conditions, scintillation can be measured with a detector recording the intensity changes over time of the radiation. The variance of the normalized intensity then allows us to measure the scintillation strength as follows:

$$\sigma^2(I/I_o) = \langle (I/I_o)^2 \rangle - \langle I/I_o \rangle^2$$

$$= [\langle I^2 \rangle - \langle I \rangle^2]/I_o^2$$

$$= \frac{\sigma^2}{I_o^2}$$

where $I = I(r,t)$, the intensity at the detector, at time t

$I_o = \langle I(r,t) \rangle$, the ensemble average

$\sigma_I^2 = \langle I^2 \rangle - \langle I \rangle^2$, the variance

It has been shown [Ref. 1] that, for the weak turbulence region, the log intensity is also a normal random variable. We can then describe scintillation strength in terms of log intensity variance. The average intensity value then does not enter into the problem. Only the log intensity variance, σ_ℓ^2, is of importance in describing the distribution. Since the intensity is proportional to the square of the amplitude, the log intensity is then proportional to 4 times the log amplitude. Eqn 1.1 can then be rewritten for log intensity variances.

$$\sigma_\ell^2 = 4\sigma_A^2 = 4\ A\ K^{7/6}\ C_n^2\ L^{11/6}$$

These fundamental relations derived by Tatarski require a weak, homogeneous turbulence of the Kolmogorov form. A

crucial assumption in this and in preceding work, [Ref. 2], [Ref. 3], is that we satisfy this condition.

If the turbulence is not constant along the propagation path, there must be some weighting for position. The direct path scintillation is thought to be reasonably well explained, with the theory in reasonable agreement with experiment. The case of the folded path scintillation is not as well understood.

Optical scintillation on folded paths was investigated at NPS in a doctoral thesis by Ze'evi [Ref. 4]. In his work, Dr. Ze'evi proposed the following path weighting functions for spherical waves, assuming a flat mirror is used for folding, and weak, Kolmogorov turbulence.

$$\text{direct path:} \quad W_L(x) = (x(1-x))^{5/6}$$

$$\text{folded path:} \quad F_F(x) = (x(2-x))^{5/6}$$

where

$x = z/z_o$

z = distance along the path from the detector

z_o = distance between detector and mirror, (folded path), or, distance between detector and source, (direct path)

In our experimental set-up, z_o was 61 meters for both paths. We stress this point to make sure the system arrangement is understood. The form of these functions is plotted in Figure 1.

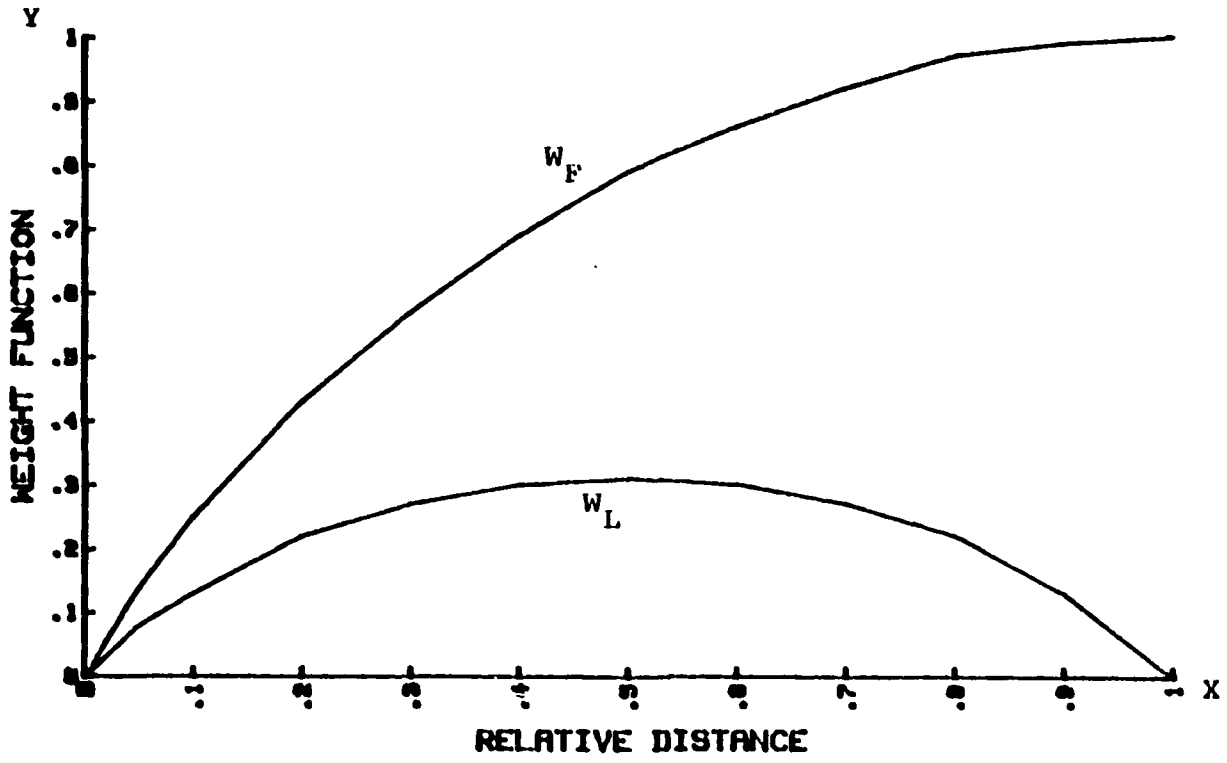

Figure 1. The weight functions of spherical waves in the cases of a single path (W_L) and a folded path with $\theta = 0$ (W_F). x represents the relative location along the path. For single path; the source at $x = 0$ and the detector at $x = 1$. For folded path; the source and the detector are at $x = 0$, the mirror is at $x = 1$.

Some work has already been undertaken at NPS to test the Ze'evi predictions [Ref. 2], [Ref. 3]. Preliminary results, although not exact fits, were encouraging. The aim of this experiment is to test the Ze'evi path weighting functions using a corner cube reflector, and to compare the resulting scintillation with that of a flat mirror.

II. EQUIPMENT

Because of previous work in this area, most of the optical and data processing equipment required for these experiments was already in existence. We made only minor modifications to existing set-ups as the research progressed. In the following sections, we briefly describe the major components of the scintillation measuring system.

A. TURBULENCE CHAMBER

In an effort to control the turbulence effects of the atmosphere on the laser signal, Costantine and Flenniken [Ref. 3], [Ref. 5], constructed a 61 meter controlled turbulence region enclosing the optical path. The "tunnel" was constructed from standard plywood sheets and consisted of 25 sections, each 2.4 meters long, by .61 meters square. These hollow boxes were joined together with masking tape, forming a closed system that was then securely taped to the tables under which the optical equipment was housed. All lasers and optics, the detector, and the entire beam path were enclosed within one volume, protected from outside disturbances.

The turbulence in the system was introduced by a heater placed in a modified tunnel section. The heater itself was a wire bent into a series of "V"'s. A variac provided a constant 70 volts to the wire for our heat source, resulting in a power of 140 watts. Air warmed by the wire rises, and

passes through a fine mesh screen, in order to create more uniform turbulence. The turbulent vortices then rise through the path of the laser beams, and up a baffle and chimney assembly. This heater section could be moved to any desired location in the tunnel, allowing the turbulence position to be easily varied. The heater section we employed was the same as that used by Costantine, except as modified for the last experiment. We will discuss the modification in detail as we discuss that particular trial. Figures 2 and 3 show the turbulence chamber and heater section.

In order to have some quantitative measure of the turbulence present, the temperature structure constant, C_t^2 was measured at each path position of the modified tunnel section during an experimental run. The temperature probes and thermocouple were inserted into the heater section directly over the heater and above the beam paths. A schematic of the system is shown in Figure 4. When directed by the controlling program, the HP-9825 sampled the two voltmeters and then calculated the temperature structure constant. Details of this procedure can be found in [Ref. 5]. The measured variances could be weighted for turbulence fluctuations by multiplying the measured data for a position by the ratio of the maximum C_T^2 for the run to the C_T^2 for that position. In our work we have not continued this particular form analysis, for reasons which will be discussed in Chapter 4.

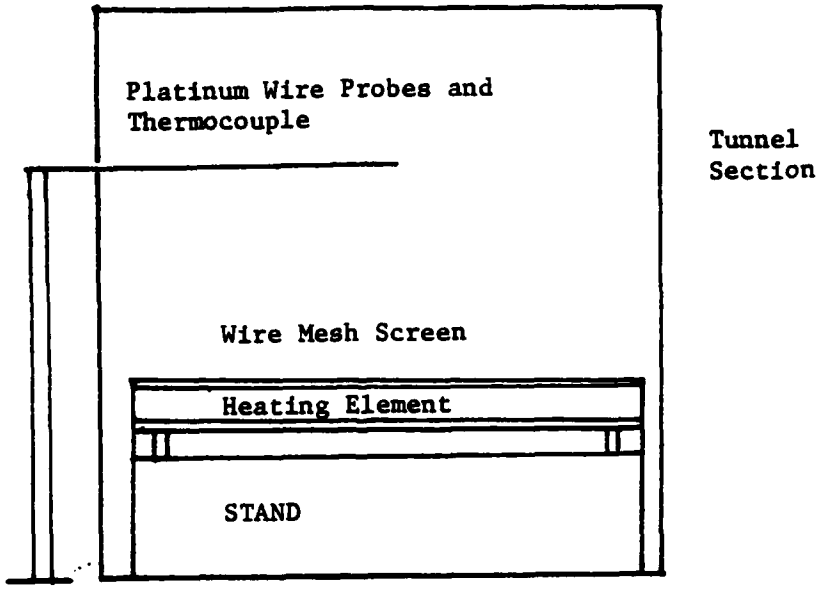

Figure 2. Heat Source, seen looking down longitudinal axis of tunnel section.

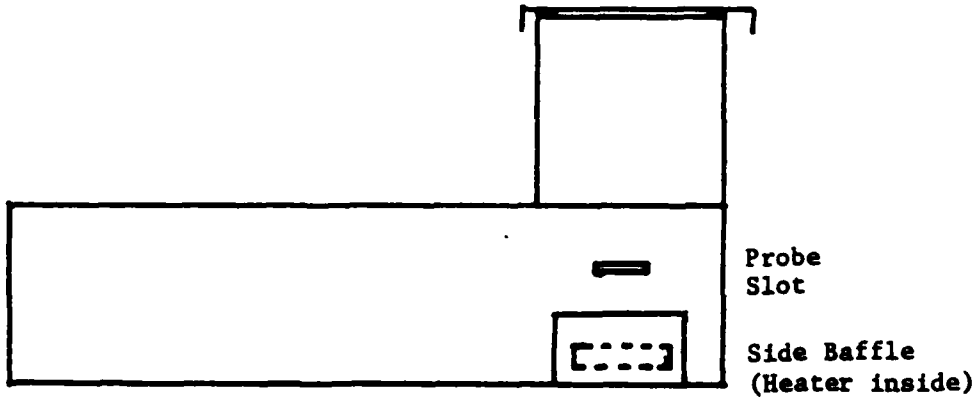

Figure 3. Turbulence Chamber, Side View.

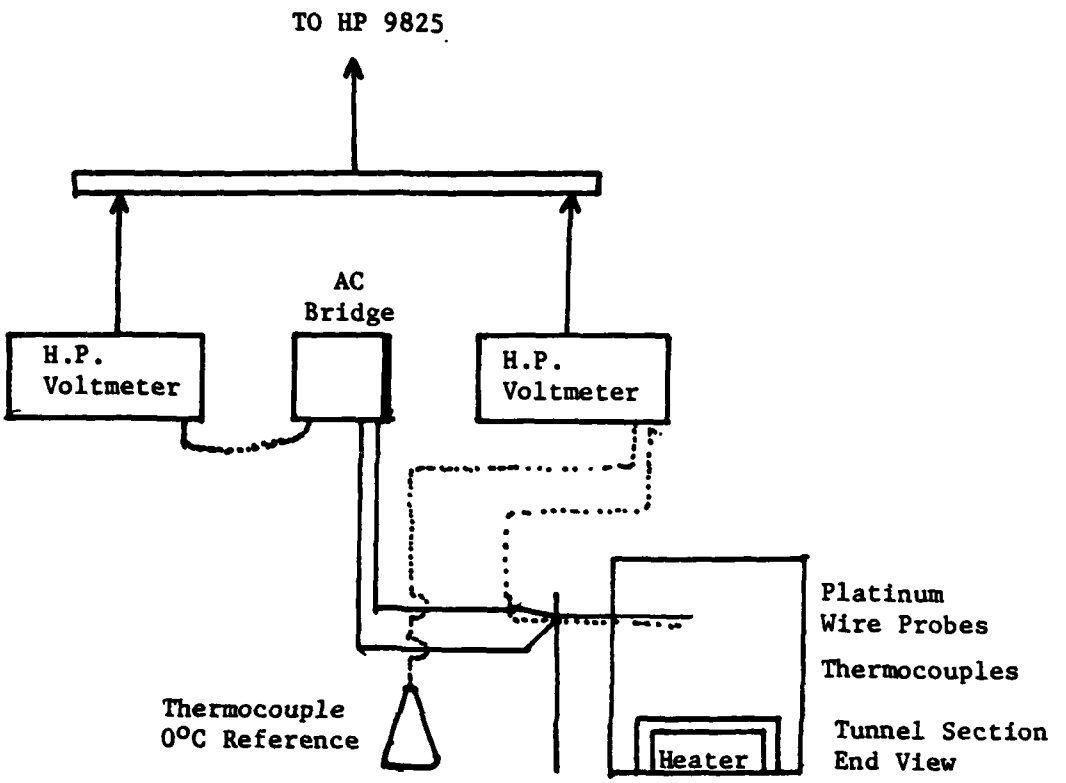

Figure 4. Schematic of C_T^2 System.

B. OPTICS

1. Direct Path

The direct path, or one way, signal originated with a Spectra Physics helium-neon laser with a .95mW output. This low power, eye-safe, visible beam offered obvious advantages in alignment and safety. The one way beam passed through a pair of polarizers enabling us to adjust the intensity of the beam as required. A convex-convex lens then focused the beam to a point at the surface of the mechanical chopper wheel. Rotating at 3000 rpm, with an open-to-close time length ratio of 1:4, the chopper provided a modulation frequency of 1 kilohertz. The chopped beam was then directed to the detector end of the tunnel by a beam splitter.

2. Folded Path

The folded path, or two way, beam begins with a laser source identical to that of the one way path. In this case, the beam is chopped by a Coherent Associates model 3003 Pockels cell and polarizer. A beam splitter directed the beam towards the reflector located behind the one-way splitter. In our experiments we concentrated on the corner cube reflector. However, the same flat mirror used by Costantine was also employed. By placing the corner cube on an optical bench, we could slide the corner cube into the beam quickly, without disturbing the much more alignment sensitive flat mirror. With this arrangement, we could rapidly switch

reflectors in the course of an experiment in order to compare the scintillation resulting from the different devices. The arrangement of the optical components is shown in Figure 5.

C. PULSE FORMING EQUIPMENT

As described above, the one-way beam was mechanically chopped. A light emitting diode and detector mounted in the chopper wheel cover were also chopped at the 1000 Hertz rate. The pulse from the LED detector provided the basis for all timing within the system. The signal from the LED triggered a function generator, which provided the actual pulses for system timing. A pulse delayed approximately 4 milliseconds was used to trigger the Pockells cell. This provided the means of chopping the two-way beam. Thus the detector was time shared between the two path signals.

This represents an important feature of this experimental set-up, in that both laser beams traverse the same atmosphere, and experience the same turbulence, at the same time. Therefore we can compare the scintillation for the different paths, since they both undergo the same effects.

D. DATA COLLECTION AND REDUCTION

We now describe the collection of the data, and its subsequent processing.

1. Data Collection Equipment

The optical signals were detected by an RCA silicon avalance photodiode, then amplified by a Princeton Applied

Research model 113 amplifier. The high and low frequency roll-offs for the amplifier were carefully adjusted to allow the signal to be amplified without creating any distortions of the signal.

The amplified signal then went to two demodulators. These devices, built at NPS, sampled the incoming pulses and prepared the raw signal for processing in the following manner: the peak return was held and then sampled; the background was sampled; the difference of these two levels taken; the result passed to a log converter. Each demodulator was triggered so that it processed signals from only one path. The output of the log converters was passed to the data reduction system, via an electronic switch that alternately offered direct or folded path data to the data reduction equipment.

2. Data Reduction Equipment

The input to the data reduction equipment was the single analog to digital converter input to the Nicolet Instruments Company NIC-80 data processor. This device took the analog voltage proportional to the log intensity fluctuation, digitized it, then stored it in the appropriate memory block. Four sets of 16384 samples each were taken for each path direction, at each heater position during an experimental run. The NIC-80 built a histogram of number of counts versus log signal intensity. The program is available in [Ref. 2]. These results were transferred to the Hewlett Packard model

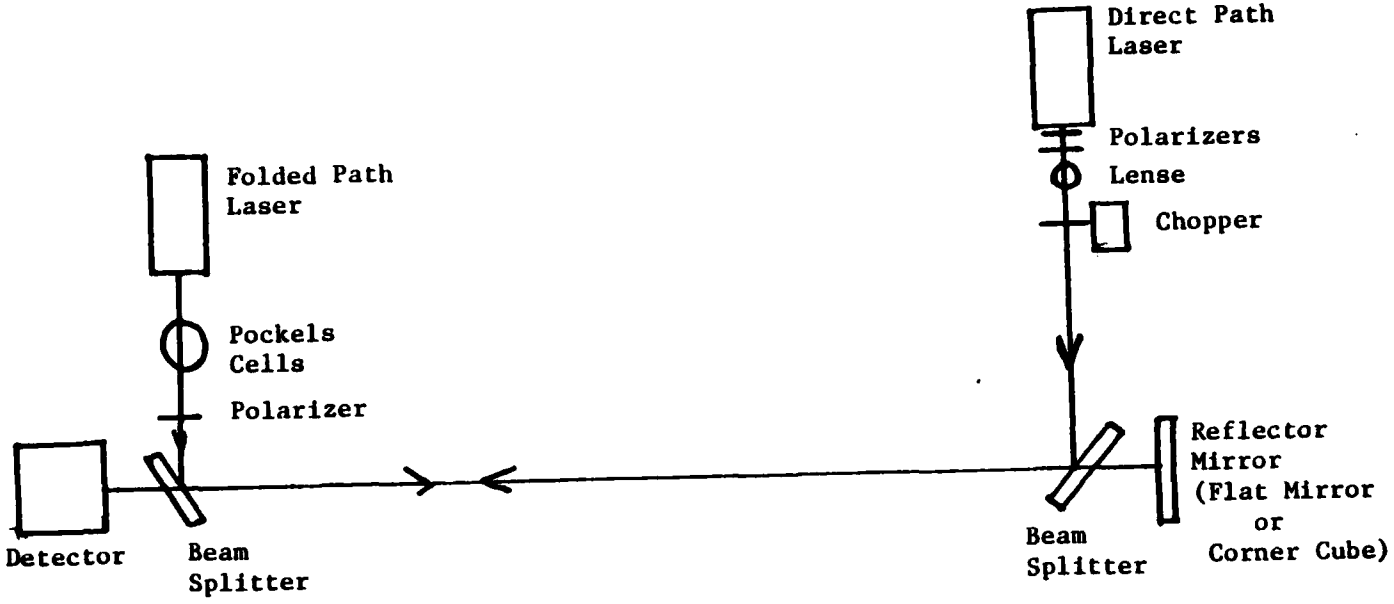

Figure 5. Arragnement of Optical Equipment.

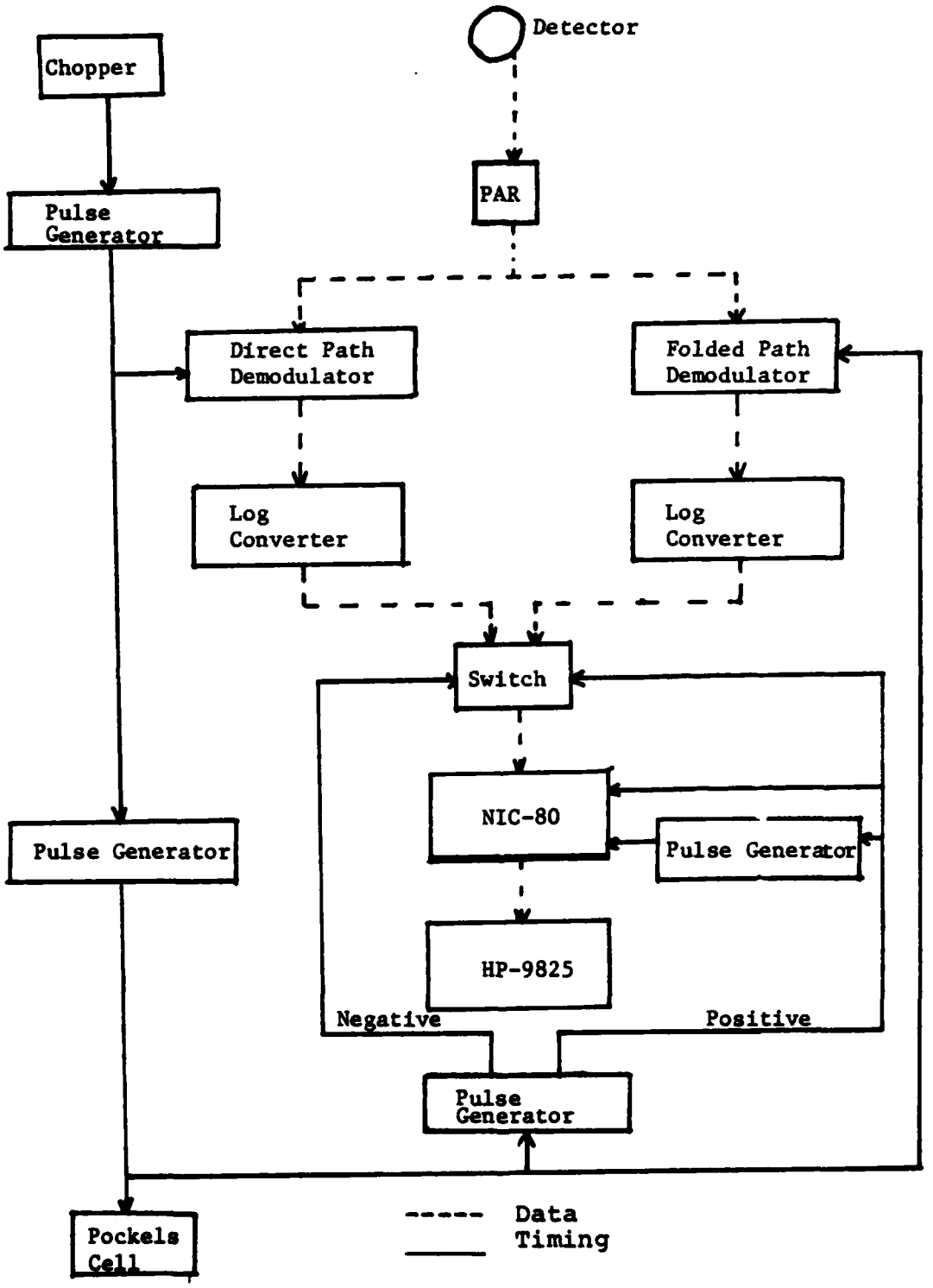

Figure 6. Block Diagram of Timing and Data Signals.

9825B computer, which was the overall controller for the experiment. Data transferred from the NIC-80 was stored on magnetic tape, then the mean and standard deviation of the distribution were calculated. The control program is also available in [Ref. 2].

The program output included an identifying header, which listed date, time, heater position, and any comments, such as PAR gain, low and high frequency roll-offs, detector high voltage, and whether an aperture was in place or not. The actual data included number of points, the standard deviation sigma, a CHI-SQUARED test parameter, and in later experiments, a fitted sigma. All of this information was arranged in columns, with a particular row pertaining to one direction of one of four trials. The rows alternated between direct and folded path data. The CHI-SQUARED test developed by Speer and Parker [Ref. 2] tests the hypothesis that the data is normally distributed. If the value of the parameter is less than 288.7, then to a 95 percent confidence interval, the hypothesis that the distribution of intensities is normally distributed is correct. Distributions which do not meet this hypothesis are marked with asterisks (**).

Plots of the intensity distributions were also made for selected points during an experiment. These plots, and the tables described above are included in the appendices giving the results of each of our experiments.

III. EXPERIMENTAL WORK

A. PROCEDURE

Our research consisted of five separate experiments, all following the general procedure used previously by Costantine [Ref. 3]. Any differences between the procedures are noted in the discussion for that particular trial.

The usual routine for an experiment required us to first assemble the tunnel sections, and seal them together with masking tape. Since the complete tunnel blocked access to labs and offices in the basement of Spanagel Hall, it was only joined together in the evening or on weekends in order to conduct an experiment. All adjacent doors were taped shut to prevent any undesired drafts into the tunnel. The detector, the laser sources, and all associated optical equipment were also sealed under the tables protecting the ends of the tunnel, so that we had a closed system. The only openings were those in the heater section, which allowed a smooth flow of air into the region directly under the heater. Warmer air would then rise up the chimney, and out a baffle arrangement intended to prevent any stray drafts from entering the system. The quiet tunnel scintillation was measured and used for a reference. Then the heater was turned on, and after warming up, the scintillation was again measured, and the outputs discussed earlier were generated. The heater tunnel section

was then untaped and relocated along the path. The procedure was repeated for each data point. The sigmas computed by the HP-9825 were used to calculate the log variance of the intensity fluctuations. The sigma for the quiet tunnel was squared, then subtracted from the sigma squared at the point. This variance was then plotted versus path position, and used to plot a least squares fit of the Ze'evi path weighting function.

B. EXPERIMENTAL GOALS

Having observed the work of Costantine we continued essentially the same experiment with the following goals in mind:

First, to gather additional data in an attempt to prove or disprove the Ze'evi path weighting theory.

Second, to use a corner cube reflector to test the theory for other than the flat mirror case.

The corner cube was chosen because the complicated reflection pattern would be a first approximation to more realistic optical systems. In addition, we suspected that the corner cube would exhibit less scintillation than the flat mirror for the same turbulence. Rays to and from the flat mirror traverse essentially the same turbulence, while rays from the corner cube are displaced from the incident ray and therefore experience slightly different turbulence. These atmospheric inhomogeneities could be considered as lenses with different focusing characteristics. A ray reflected

from the flat mirror passes through the same lense twice. A ray reflected from the corner cube passes through two different lenses, each with different focusing or defocusing characteristics.

C. EXPERIMENTS

We now examine the results of this work.

1. 12 May Experiment

In this experiment, the flat mirror reflector was replaced with a corner cube having a 6.8 centimeter diameter. Data was collected at thirteen heater positions, 1.0, 5.8, 10.7, 15.5, 20.4, 25.3, 30.1, 35.0, 39.8, 44.7, 49.5, 54.4, and 60.0 meters, measured from the detector end. Least square fits to the results are plotted in Figures 7 and 8, while the complete data is listed in Appendix A.

Both the direct and folded path results showed trends seen in the previous work by Costantine with a flat-mirror reflector. The two-way variances exhibited step-like behavior as the heater approached the reflector end of the tunnel. The one-way variances had an unexpected drop near the center of the path. We are at a loss to explain the jump at the 54.4 meter position for both the direct and folded paths.

2. 19 May Experiment

For this trial, we modified the reflectors as discussed earlier. The corner cube could be moved quickly in or out of the beam path, without disturbing the flat mirror, enabling us to switch between reflectors during the experimental

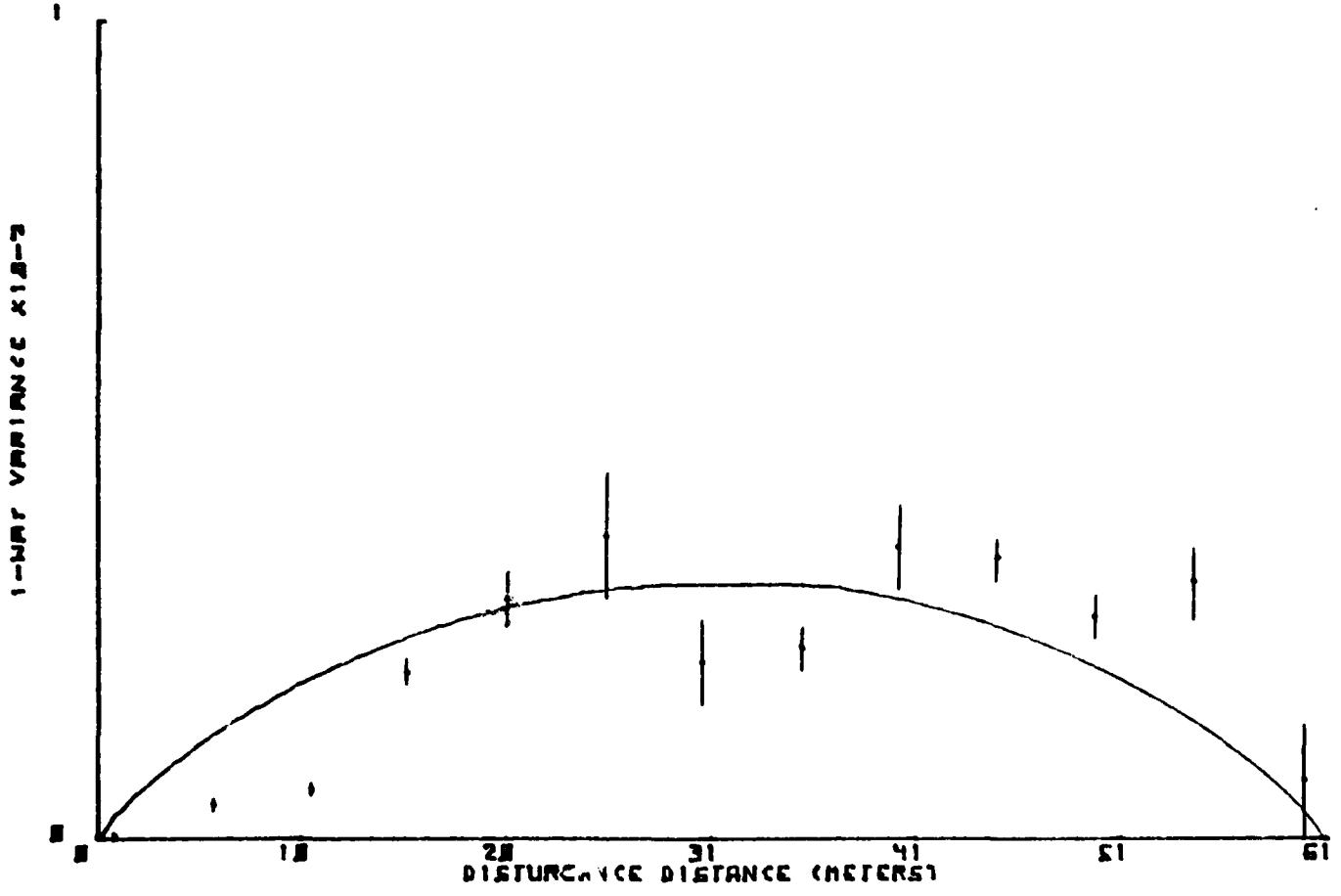

Figure 7. Least Squares Plot of Corner Cube, Direct Path Variance Versus Distance From Detector for 12 May 1983 Experiment. Solid Line Represents Ze'evi Path Weighting Function.

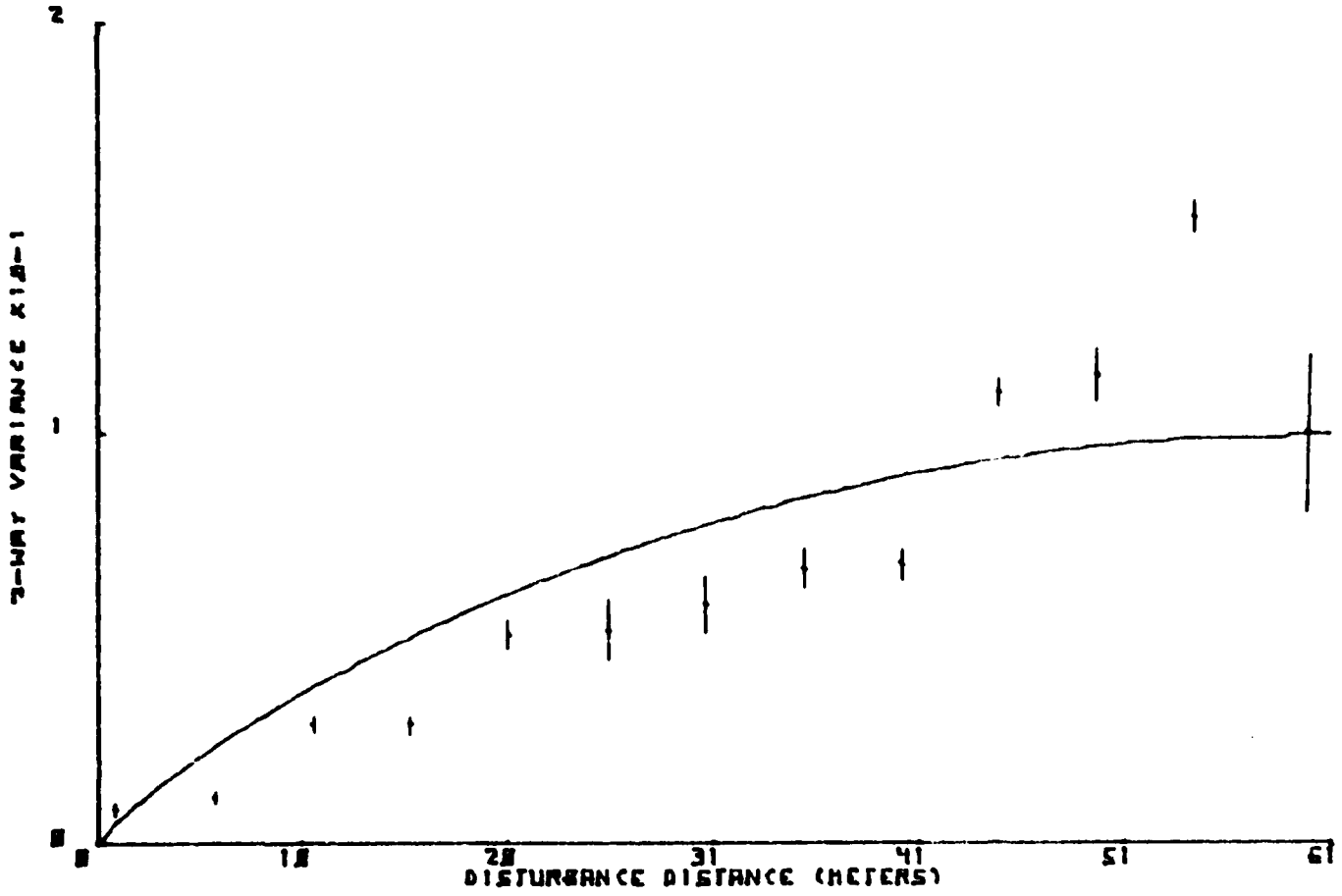

Figure 8. Least Squares Plot of Corner Cube Folded Path Variance Versus Distance From Detector for 12 May 1983 Experiment. Solid Line Represents Ze'evi Path Weighting Function.

run. When not in use the flat mirror was covered to remove the possibility of any spurious reflections. Similarly, the corner cube was covered and moved to the end of the optical bench while the flat mirror was used. It was thought that this approach would allow for better comparisons between flat mirror and corner cube reflectors.

The same 13 path positions were to be used, however only 8 were completed. The high voltage power supply for the detector began to malfunction, generating interference in the output signal. Thus, we were forced to stop at the 20.4 meter position.

It should be pointed out that this alternating reflector procedure was essentially two experiments in one, thus doubling the time required for the run. Figures 9, 10, 11 and 12 show the experimental results, with the detailed data in Appendix B. Once again the folded path shows the step like behavior, the direct path exhibits some dip near the center points, and an unusually high point near the reflector end.

3. 9 September Experiment

Since the last trial much of the scintillation equipment had been disassembled and used for another project. As a result, the system had to be reassembled, aligned and retested. A battery powered detector high voltage power supply was developed and tested. This battery supply solved the intermittent interference problem we had experienced with the previous power supply. A drawback, however, was the relatively

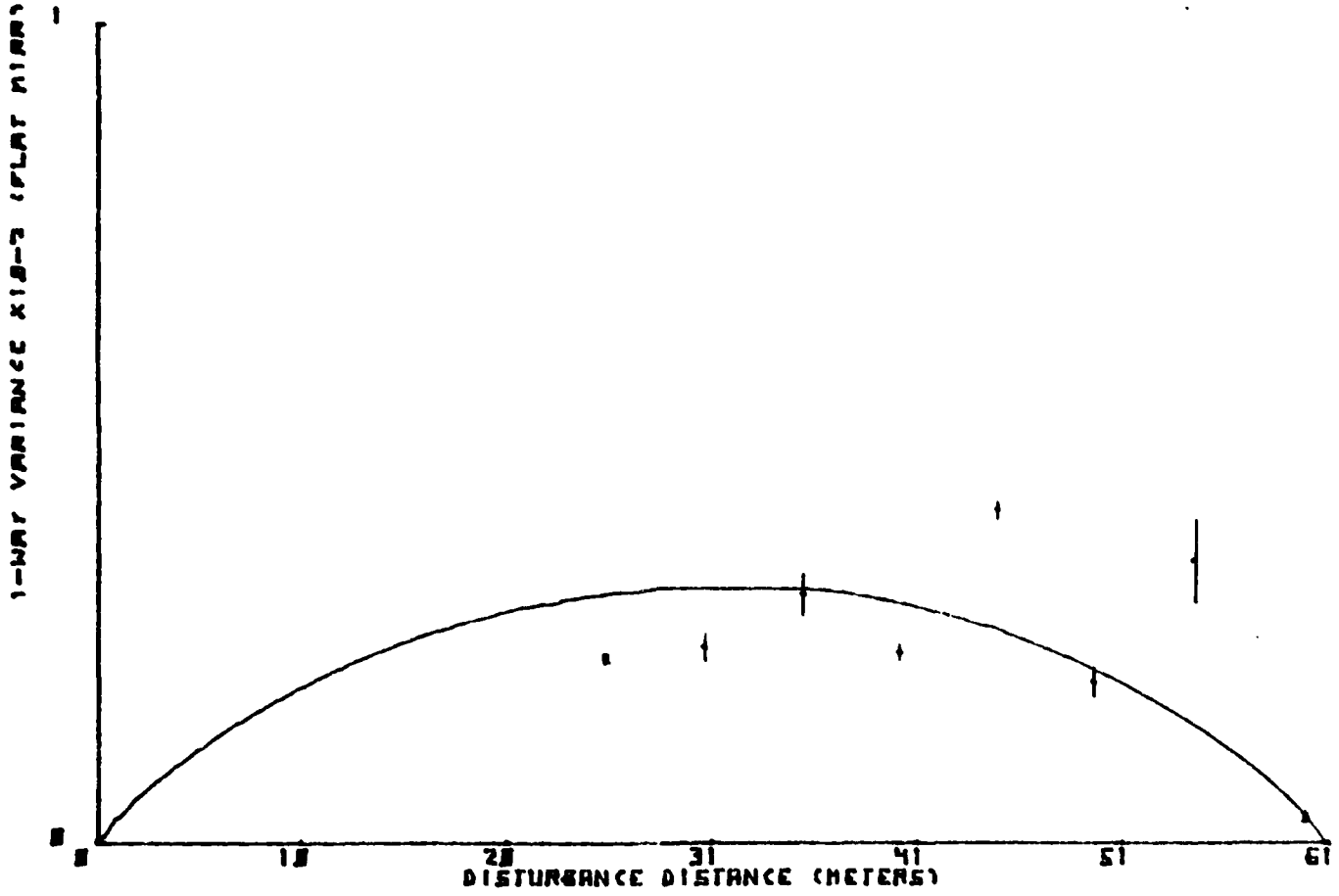

Figure 9. Least Squares Plot of Flat Mirror, Direct Path Variance Versus Distance From Detector of 19 May 1983 Experiment. Solid Line Represents Ze'evi Path Weighting Function.

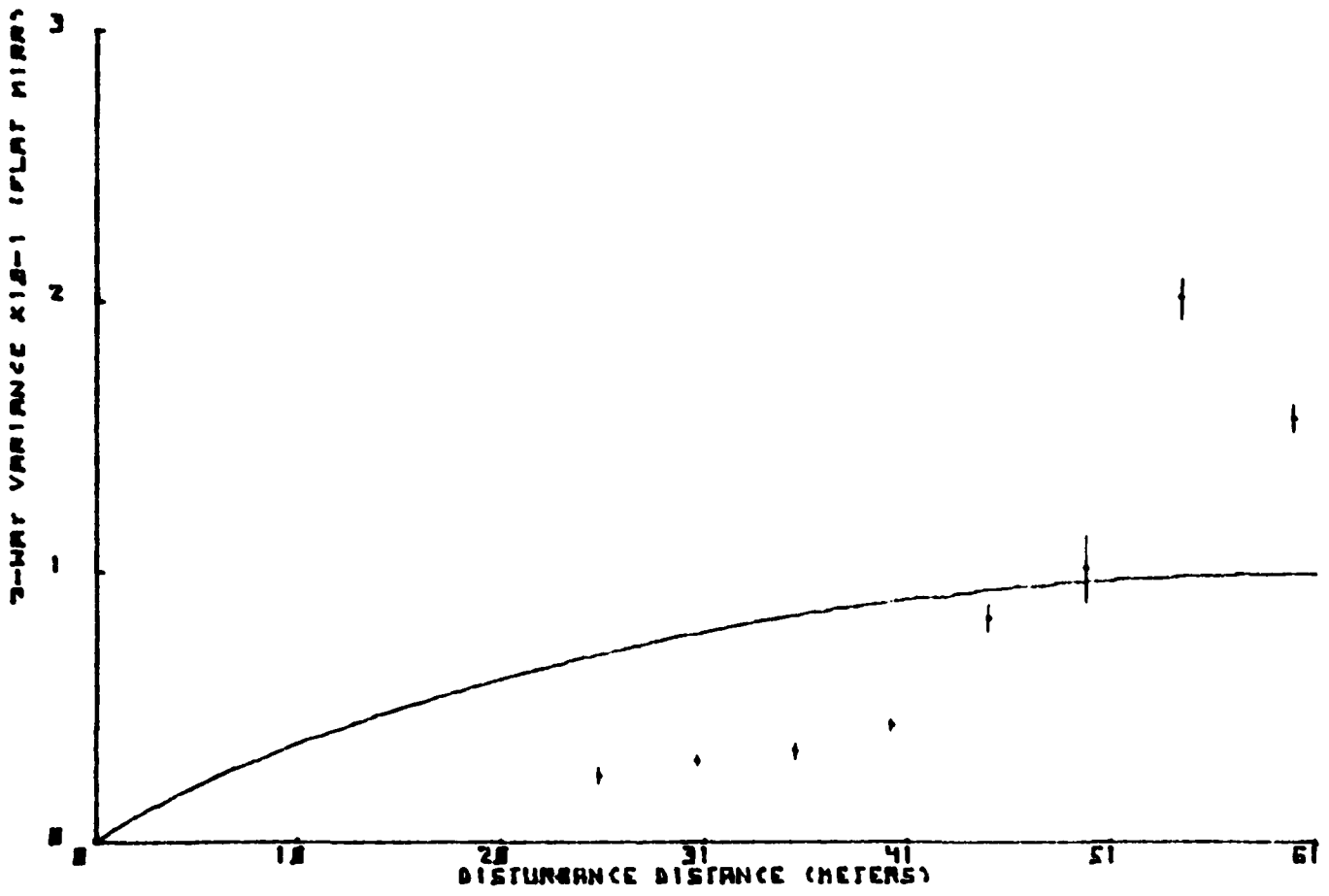

Figure 10. Least Squares Plot of Flat Mirror Folded Path Variance Versus Distance From Detector for 19 May 1983 Experiment. Solid Line Represents Ze'evi Path Weighting Function.

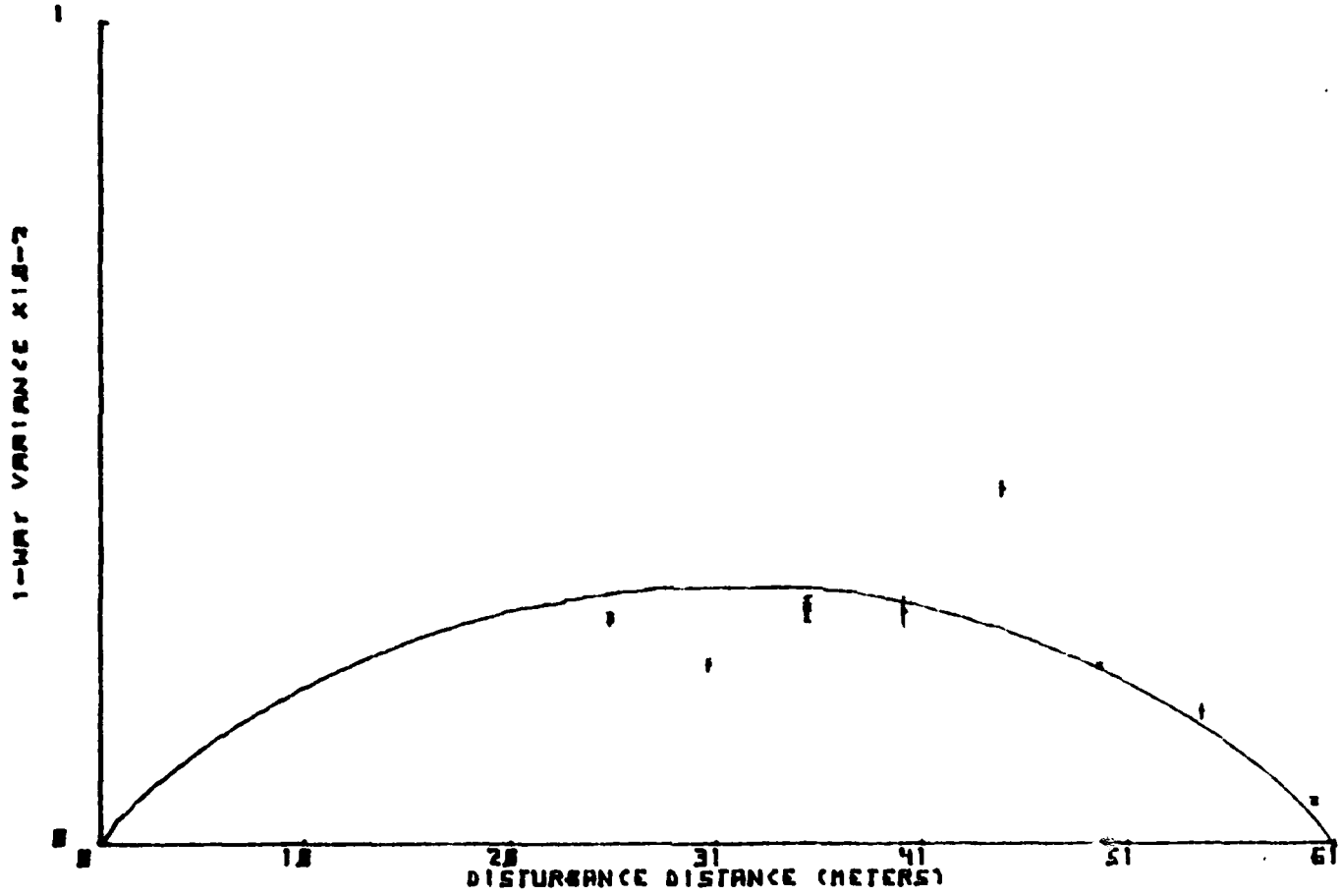

Figure 11. Least Squares Plot of Corner Cube, Direct Path Variance Versus Distance From Detector of 19 May 1983 Experiment. Solid Line Represents Ze/evi Path Weighting Function.

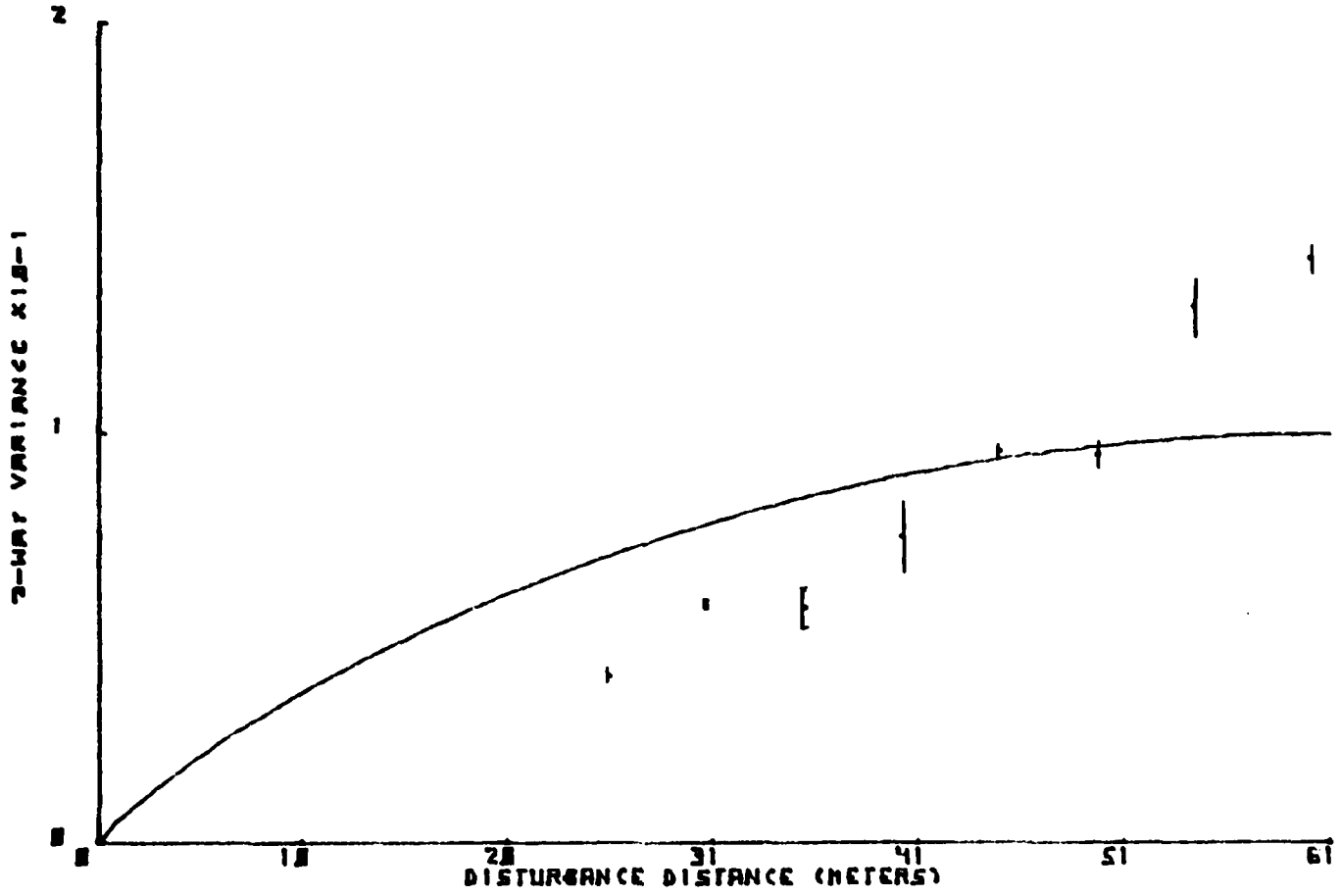

Figure 12. Least Squares Plot of Corner Cube Folded Path Variance Versus Distance From Detector of 19 May 1983 Experiment. Solid Line Represents Ze'evi Path Weighting Function.

short lifetime of the batteries at full power, requiring frequent battery changes.

In this trial we sampled nine points along the path, at 60.0, 57.6, 55.2, 52.8, 50.4, 45.6, 36.0, 24.0, and 12.0 meters. We chose to weight the reflector end more heavily because of our interest in both the two-way path in general, and the wild fluctuations we had observed in the two previous efforts.

Once again we used the alternating flat mirror and corner cube procedure. Least squares plots of the data are shown in Figures 13 through 16, with the complete results in Appendix C. We had considerable difficulty in maintaining the folded-path signal strength throughout the experiment. This we attributed to fast fading batteries, or to some alignment problem with the two-way reflectors. The real problem was revealed a few days later when the two-way laser ceased to function, after exhibiting wild fluctuations in intensity during some routine alignment work.

Once again the data seems to follow the predicted trend, but with wild scatter and anomalous jumps. For example, the previous dip near the center of the one-way path is not present, or at least not visible in the wide spacing between points.

4. 15 October Experiment

In reviewing the previous trial we decided that alternating the reflectors was not effective. The doubling of the

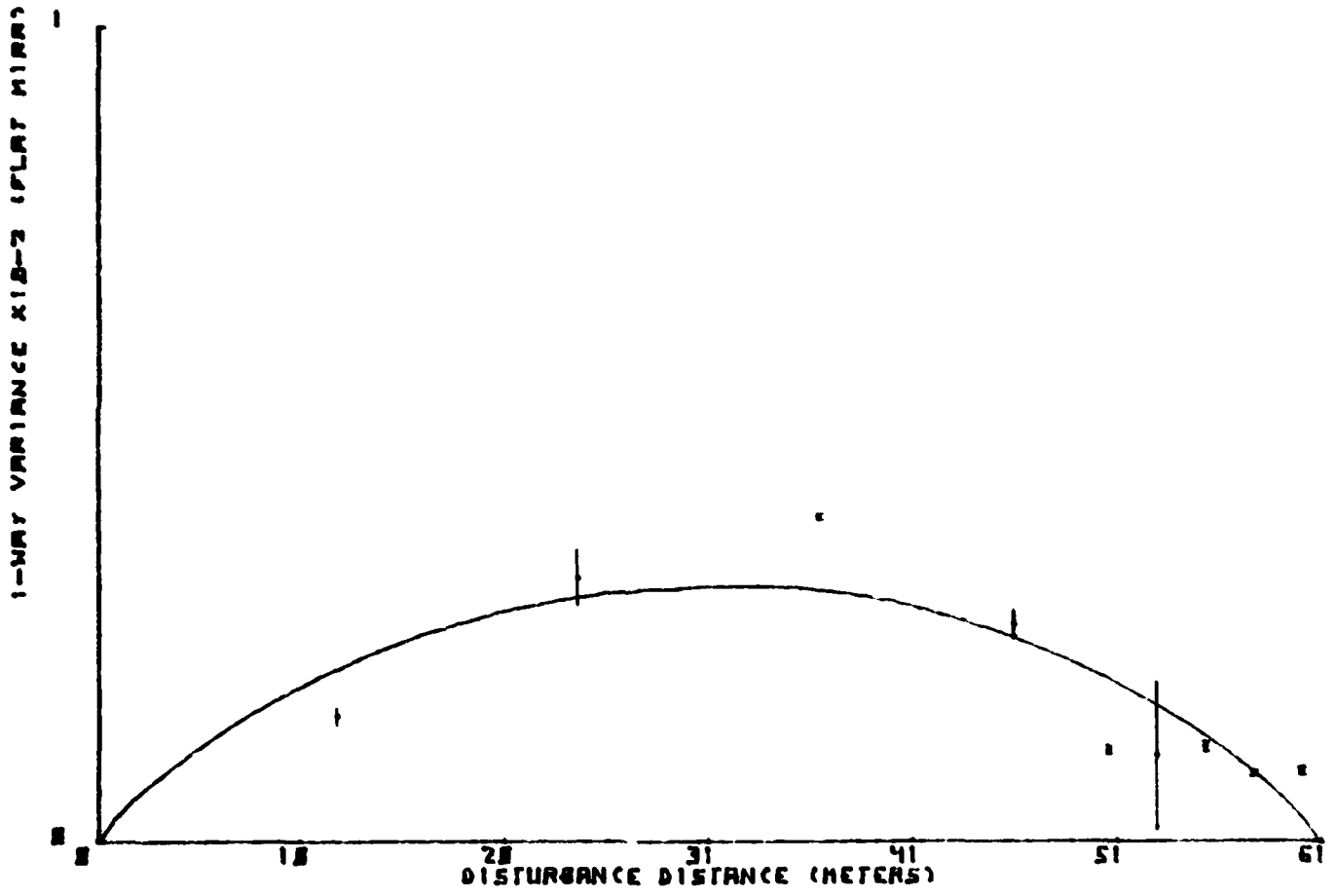

Figure 13. Least Squares Plot of Flat Mirror, Direct Path Variance Versus Distance From Detector for 9 September 1983 Experiment. Solid Line Represents Ze'evi Path Weighting Function.

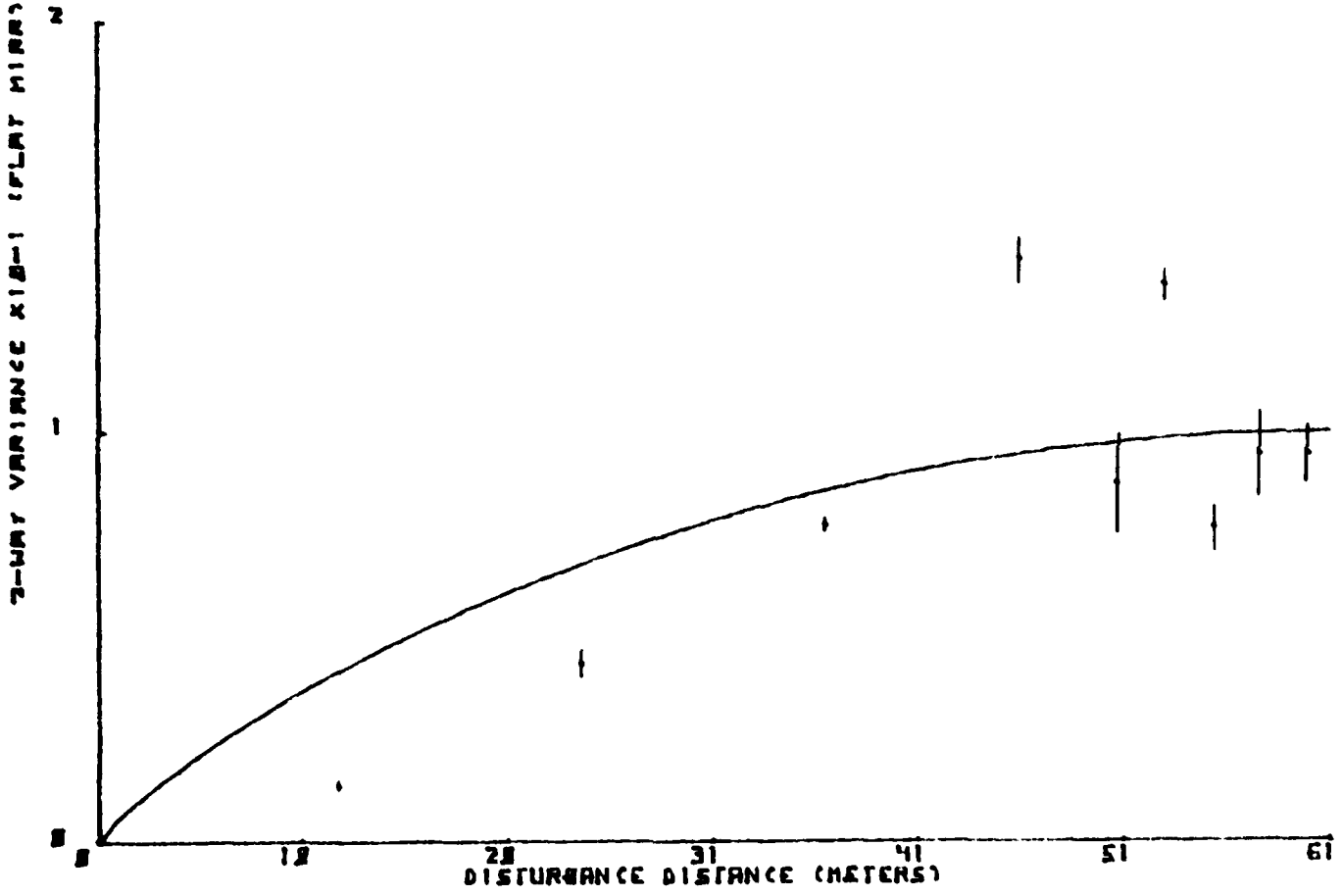

Figure 14. Least Squares Plot of Flat Mirror Folded, Path Variance Versus Distance From Detector for 9 September 1983 Experiment. Solid Line Represents Ze'evi Path Weighting Function.

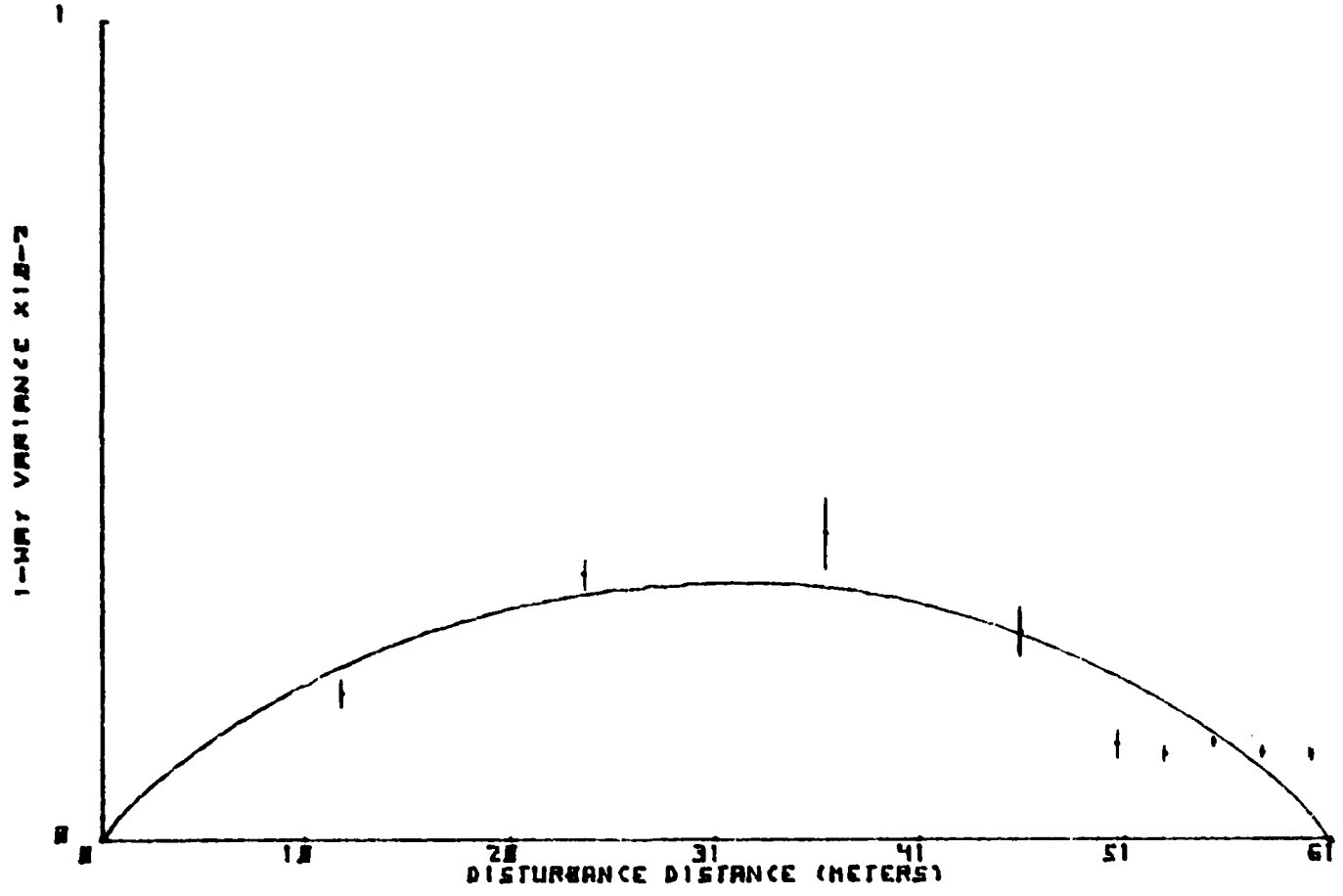

Figure 15. Least Squares Plot of Corner Cube, Direct Path Variance Versus Distance From Detector for 9 September 1983 Experiment. Solid Line Represents Ze'evi Path Weighting Function.

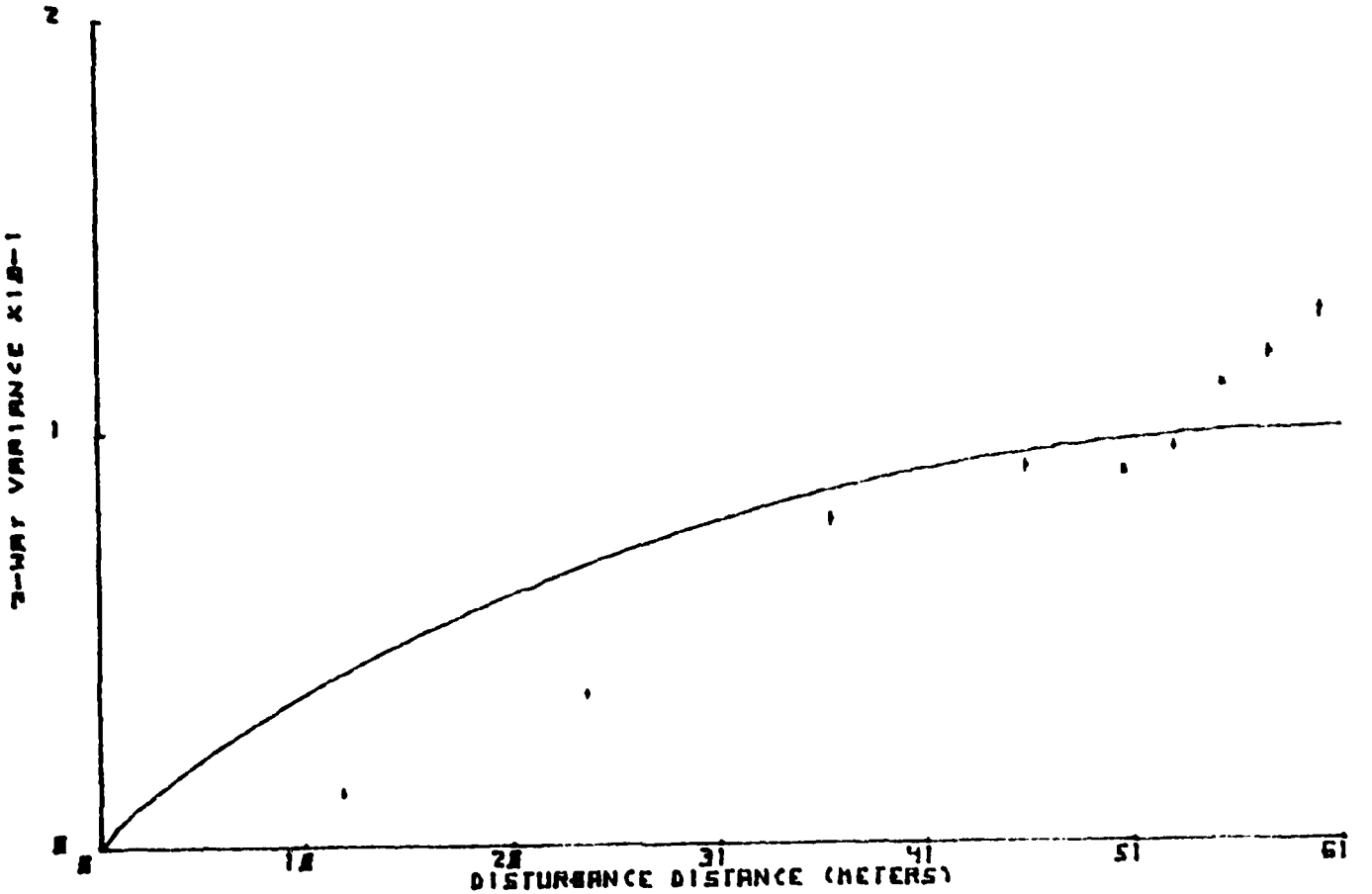

Figure 16. Least Squares Plot of Corner Cube Folded Path Variance Versus Distance From Detector for 9 September 1983 Experiment. Solid Line Represents Ze'evi Path Weighting Function.

time required for an experiment appeared to have an adverse effect on the equipment; for example, the high voltage power supply. In order to change the reflectors, the back cover of the protective table had to be removed, and the corner cube manually repositioned. Vibrations on the mirrors resulting in misalignment and intensity fluctuations were possible with so much activity close to the reflectors. For this experiment, then, we used only the corner cube. A more balanced selection of ten path positions were chosen, at 60.0. 57.6, 52.8, 48.0, 43.2, 36.0, 28.8, 21.6, 14.4, and 7.2 meters. The inoperative two way laser had been replaced, as well the detector diode. Each device was replaced with the same model as had been in use. In light of these preparations, the results were again disappointing in their inconsistency. The extreme jump in the two-way path variance was now a dip, and had moved toward the detector end. The direct path exhibited a new pattern near the detector end, remaining unusually low, then jumping wildly to a maximum at the 36.0 meter point. Least squares plots are shown in Figures 17 and 18, with detailed results in Appendix D.

5. 11 November Experiment

In reviewing all the previous work we were unable to form any strong conclusion, other than to note the marked differences between trials. Two new features were added to the system for this trial in an effort to reduce the scatter of data.

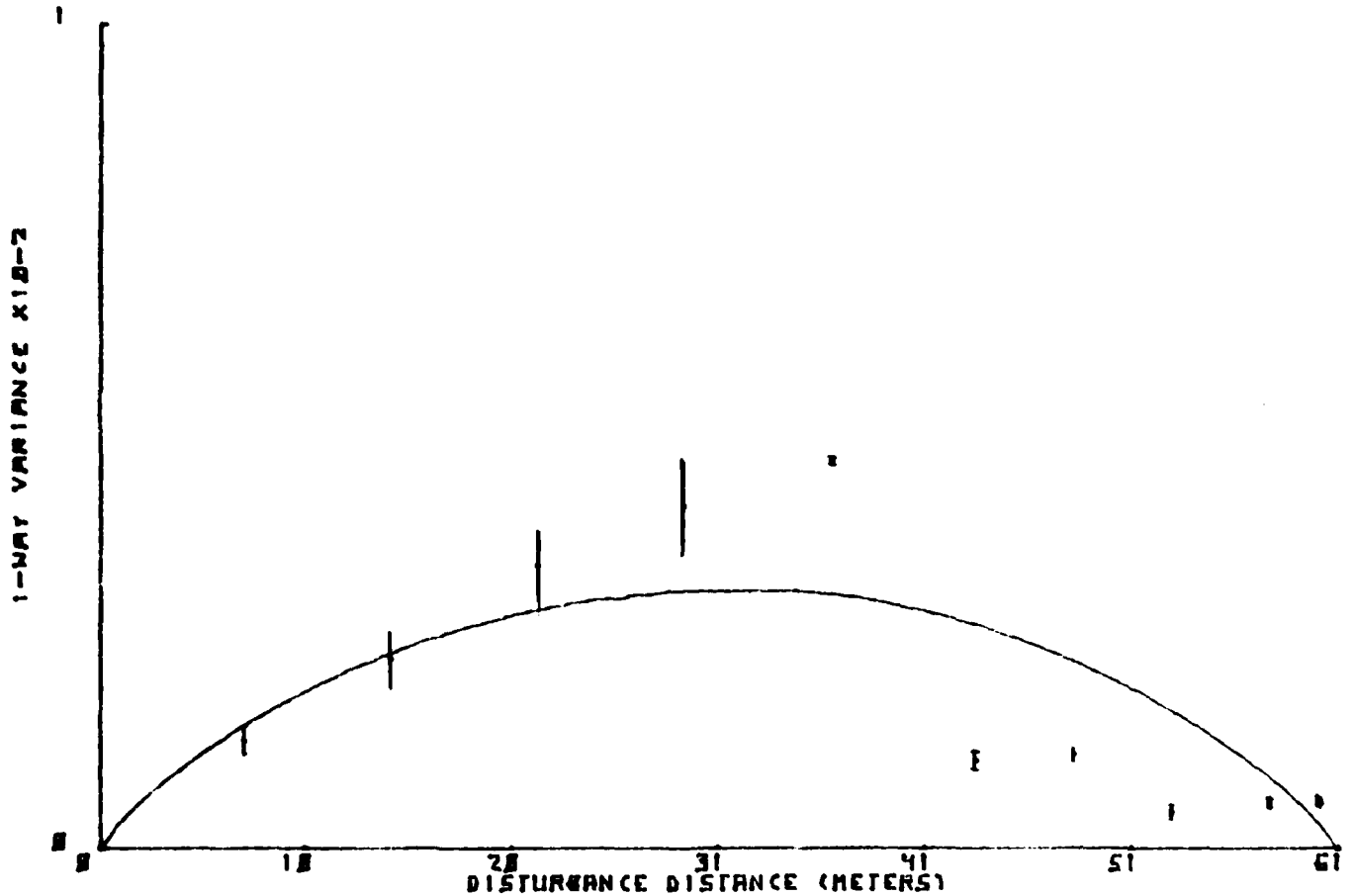

Figure 17. Least Squares Plot of Corner Cube, Direct Path Variance Versus Distance From Detector for 15 October 1983 Experiment. Solid Line Represents Ze/evi Path Weighting Function.

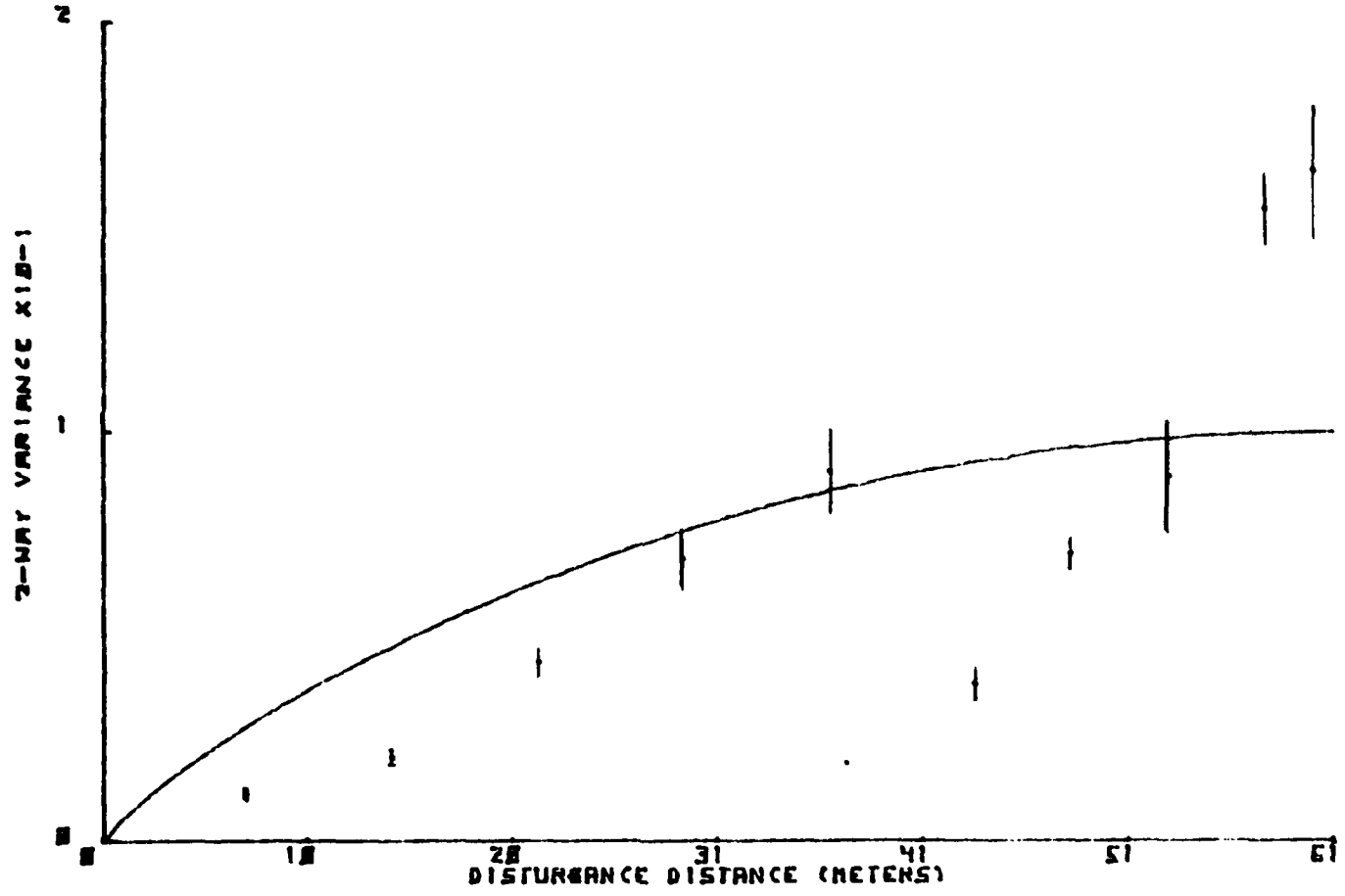

Figure 18. Least Squares Plot of Corner Cube, Folded Path Variance Versus Distance From Detector for 15 October 1983 Experiment. Solid Line Represents Ze'evi Path Weighting Function.

First an additional polarizer was inserted between the two-way laser and the Pockel's cell. This was adjusted to reduce the DC component of the signal. Our fear was that this ever present DC level, characteristic of the Pockel's cell was somehow interfering or adding to the one-way scintillation. The two-way beam now went from the laser through the first polarizer, through the Pockel's cell, and then through the second polarizer, before being directed downrange.

Our second step was to take action to create a positive flow of air upward through the beam and out the tunnel chimney. We speculated that our heater was not drawing air in smoothly from the outside, rather that it was using air from along the long axis of the tunnel. If so, this would be upsetting our assumption of a controlled turbulence source. To achieve this positive flow, we installed a fan in the roof of the chimney, directed so that it exhausted air from the heater section to the outside. In addition, two plywood baffles were installed inside the tunnel, approximately .1 meter from either side of the heater element. These baffles would act to limit the flow of air along the logitudinal axis of the tunnel. Holes of sufficient size were cut in the baffles to allow the beam to propagate without any additional diffraction effects.

The results are shown in Figures 19 and 20 and Appendix E. They show the familiar step like behavior of the two-way path, and the positive mid-point jump of the one-way path.

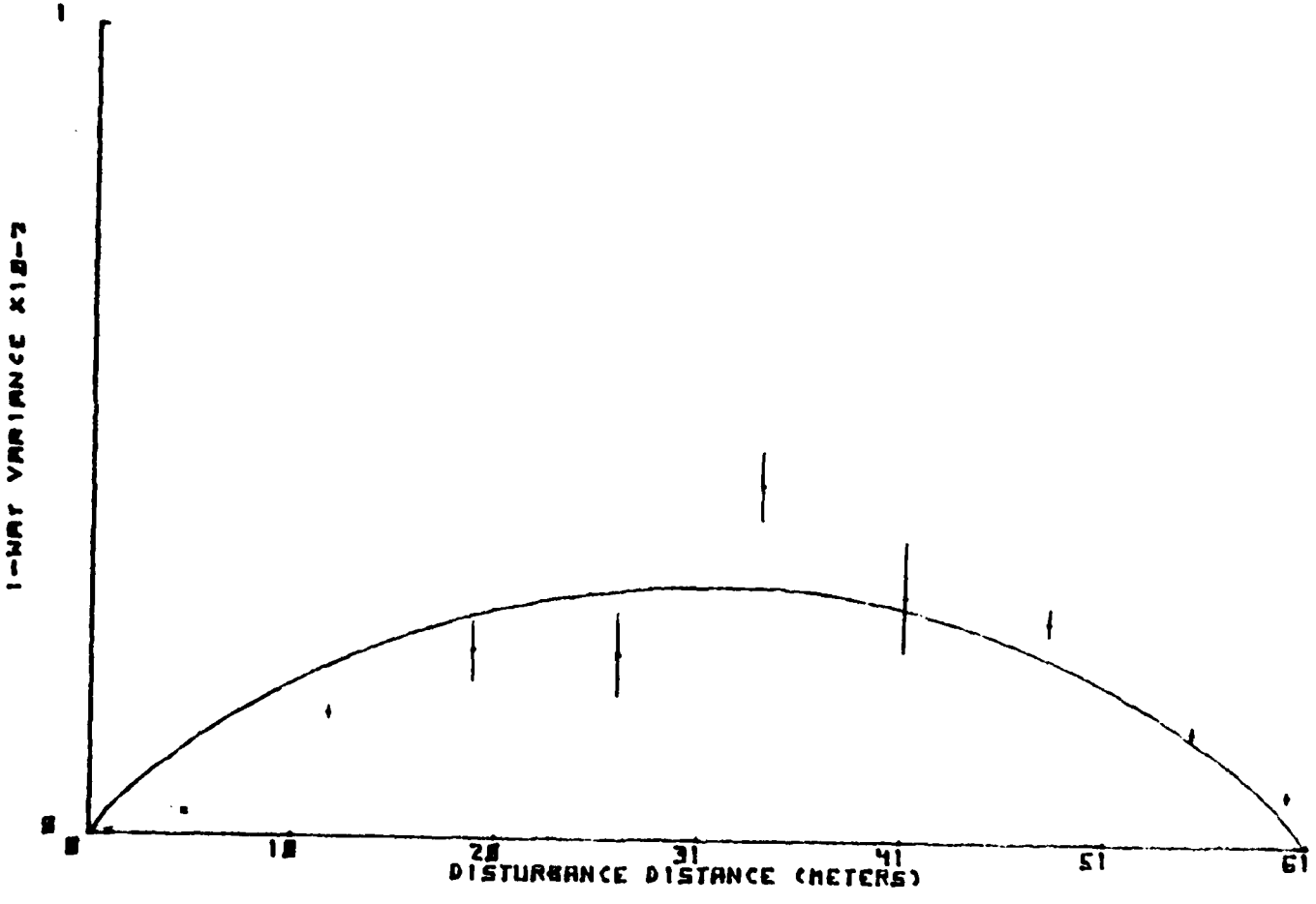

Figure 19. Least Squares Plot of Corner Cube, Direct Path Variance Versus Distance From Detector for 11 November 1983 Experiment. Solid Line Represents Ze'evi Path Weighting Function.

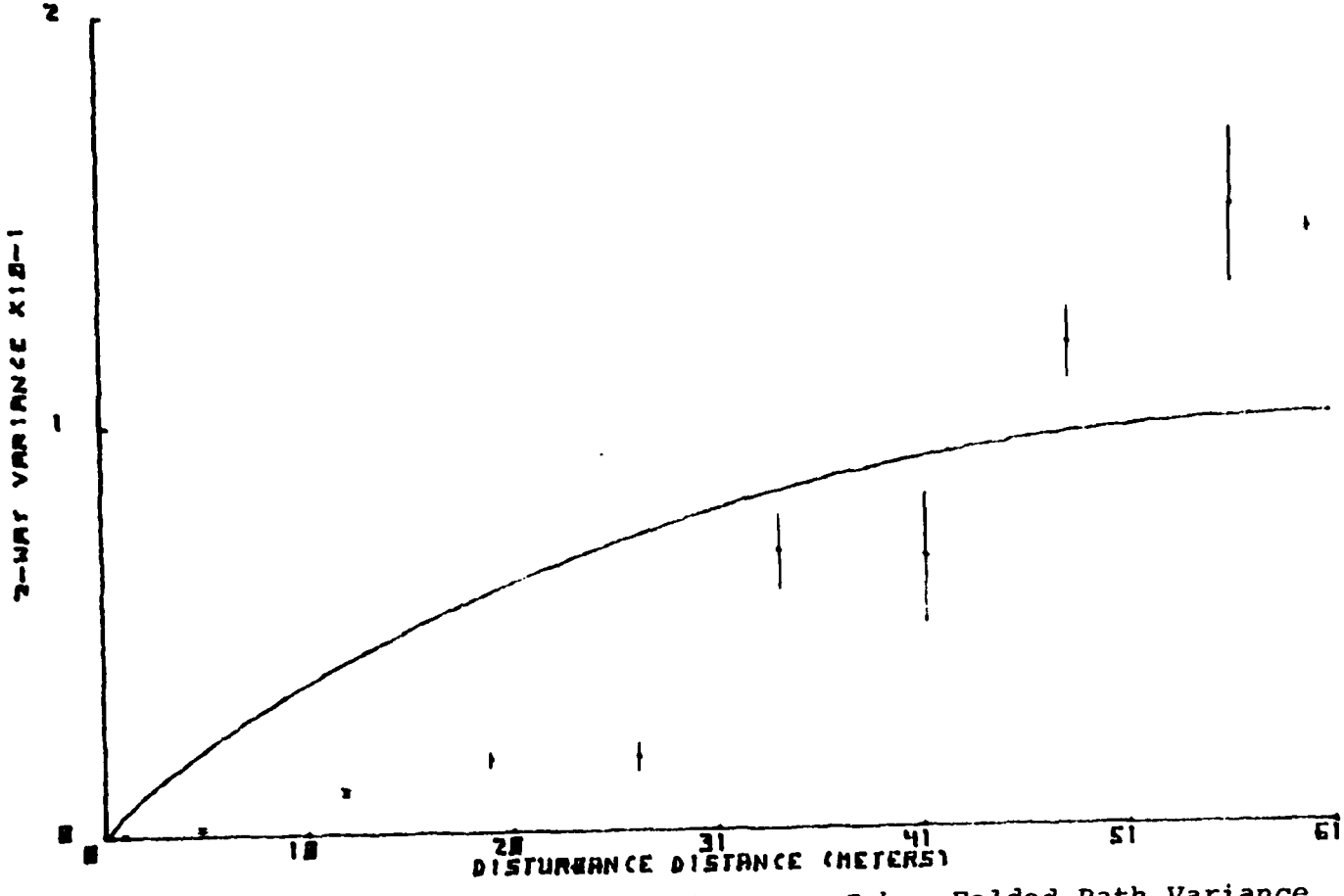

Figure 20. Least Squares Plot of Corner Cube, Folded Path Variance Versus Distance From Detector for 11 November 1983 Experiment. Solid Line Represents Ze'evi Path Weighting Function.

Cumulative plots of all data for the flat mirror, from Costantine, and the corner cube are found in Figures 21 through 24. Again, the solid line represents a least squares fit of the data points to the path weighting function. The plots show that, on average, the corner cube tends to exhibit less scintillation than does the flat mirror. Overall, these plots, as well as their predecessors, show only a poor fit to the predicted path weighting functions proposed by Dr. Ze'evi.

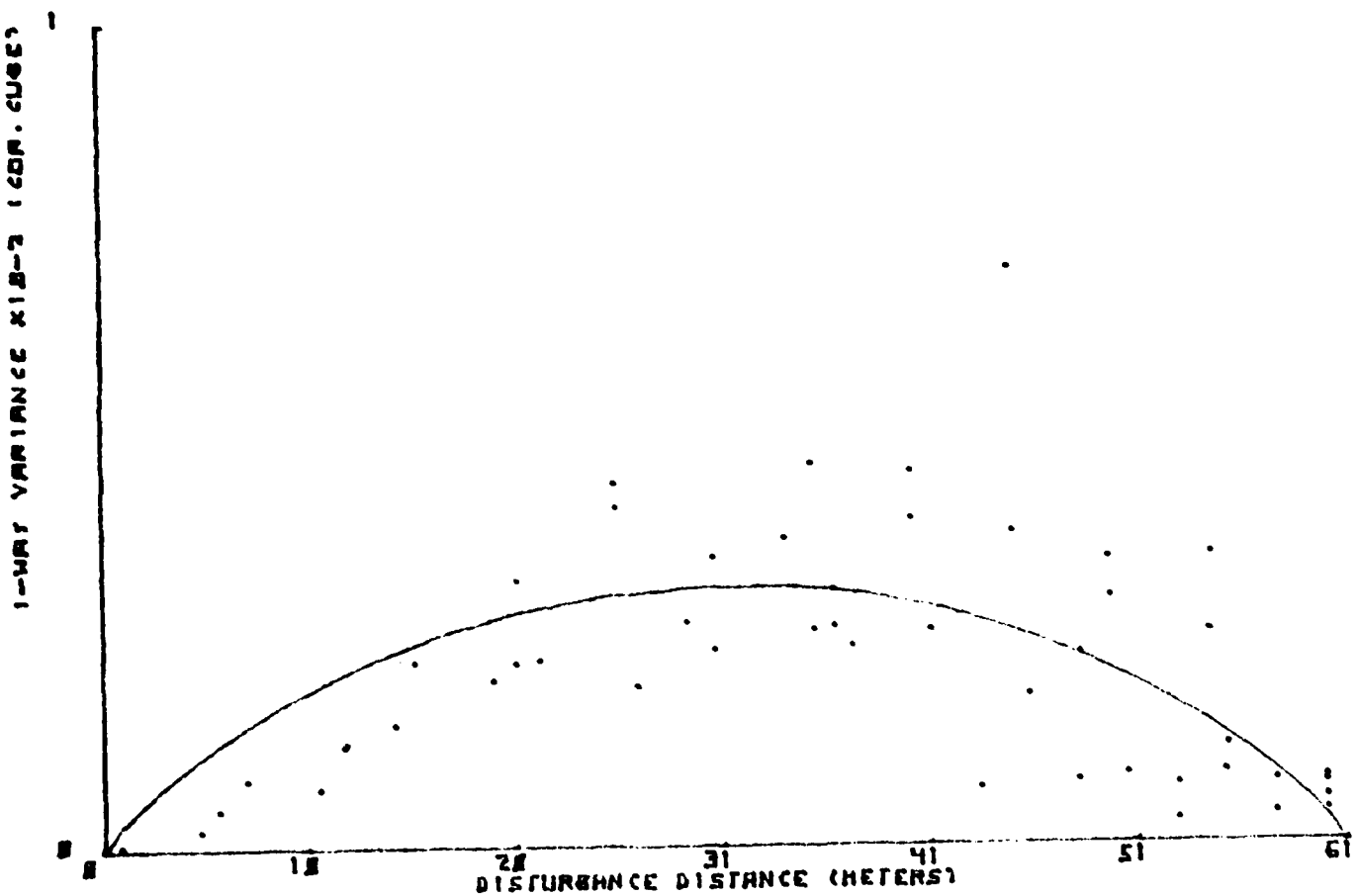

Figure 21. Cumulative Plot All Direct Path Corner Cube Data Points.

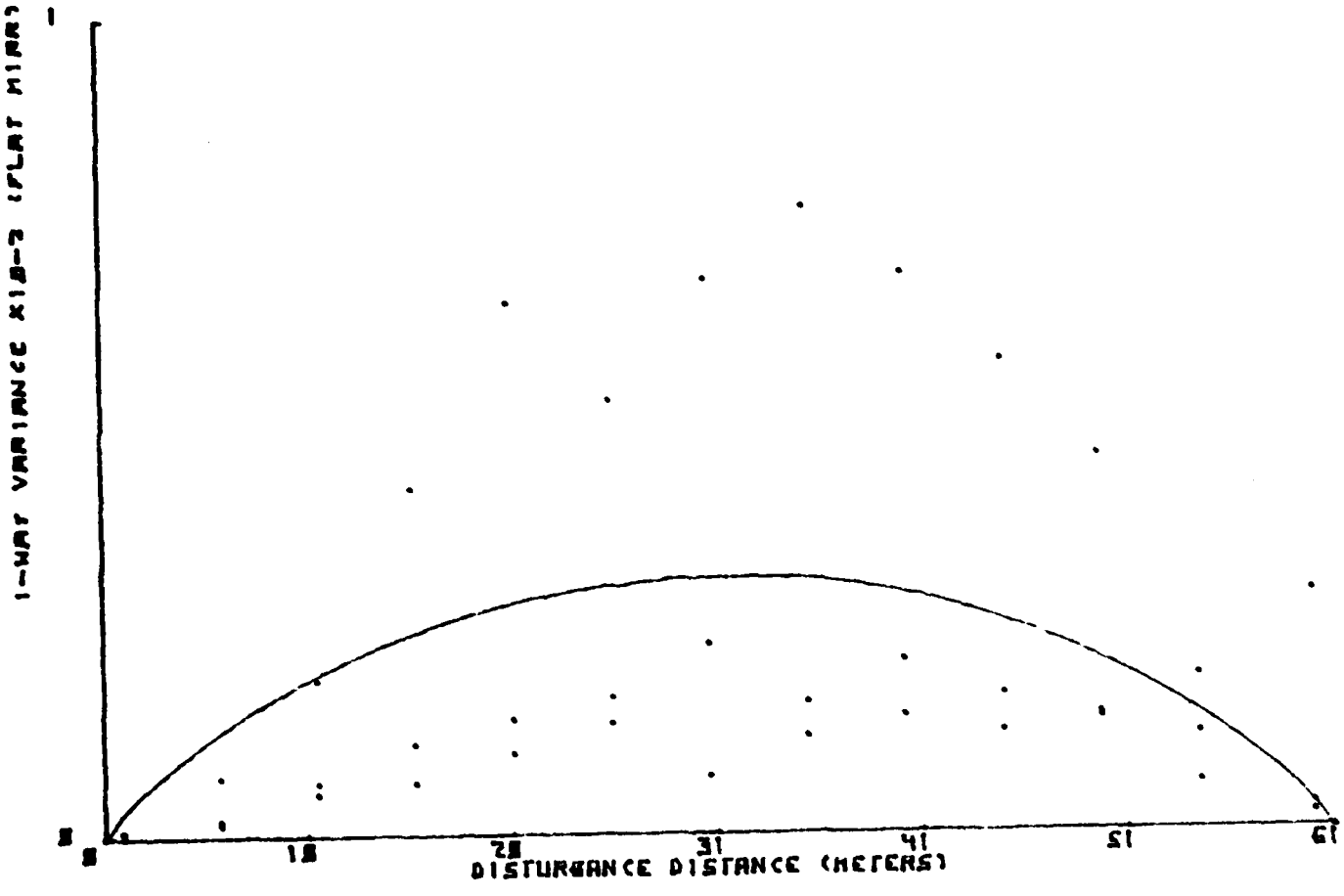

Figure 22. Cumulative Plot All Direct Path Flat Mirror Data Points, From Costantine [Ref. 3].

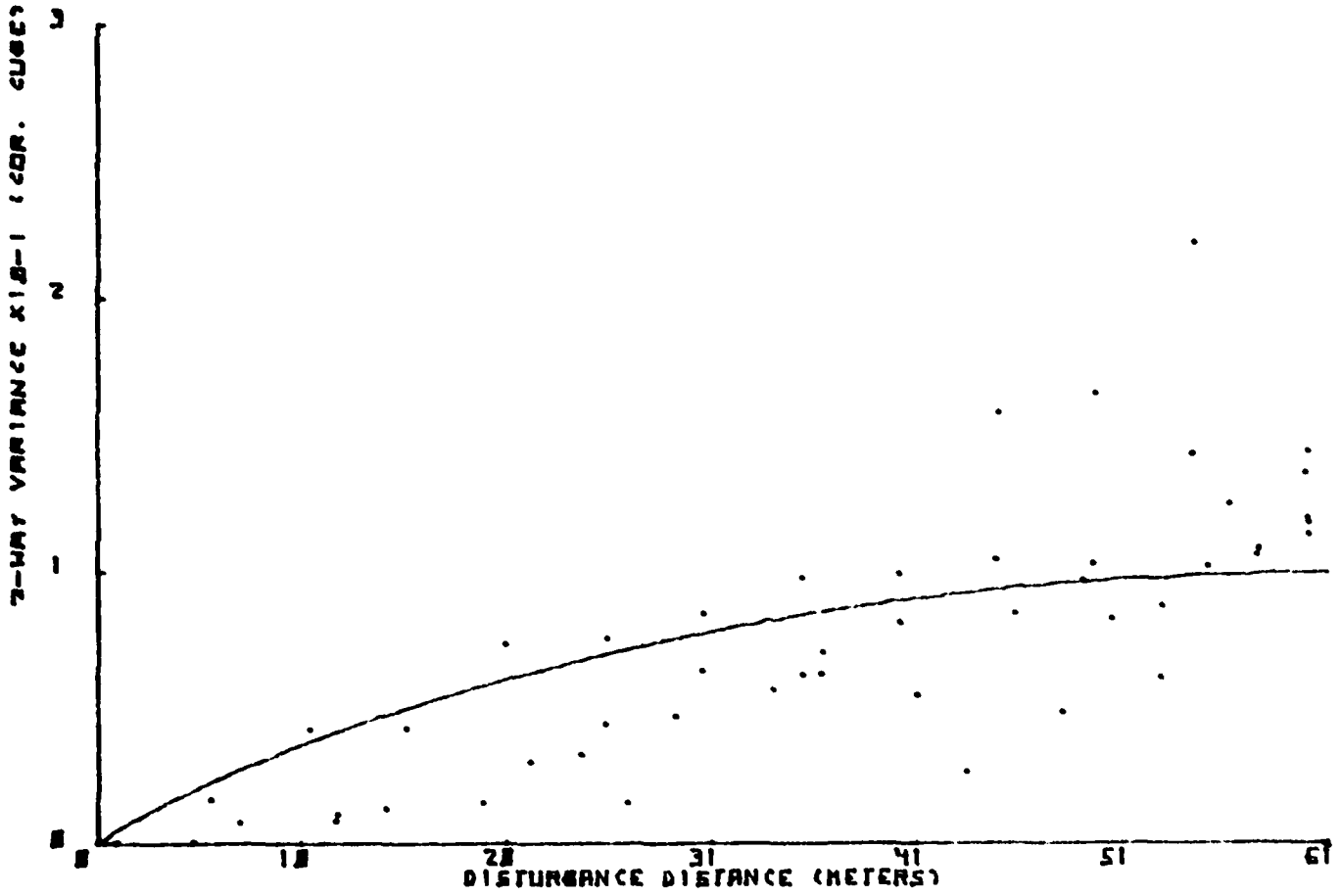

Figure 23. Cumulative Plot All Folded Path Corner Cube Data Points.

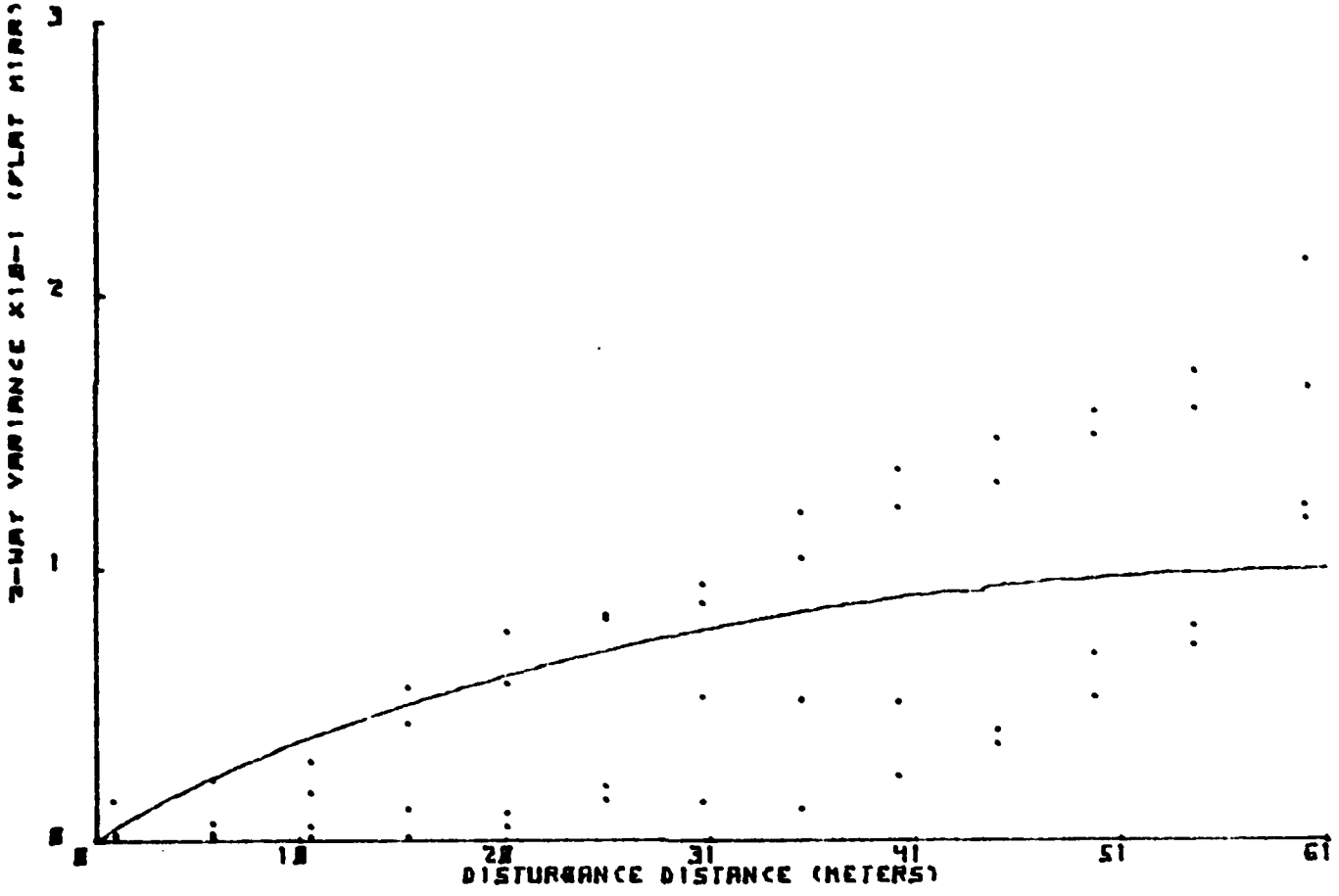

Figure 24. Cumulative Plot All Folded Path Flat Mirror Data Points. From Costantine [Ref. 3].

IV. TURBULENCE

A. BACKGROUND

In reviewing our work the corner cube, and that of Costantine with the flat mirror, some similarities were noted. For example, in the case of the folded path, the step like pattern, and the overestimation of the scintillation strength near the reflector were present for both the corner cube and the flat mirror. In light of these results, it was suggested that, in the course of an experimental run we passed from one scale of turbulence to another. If this were indeed occurring, the theory's assumptions of a weak, homogeneous turbulence would be violated. A turbulence function other than the Kolmogorov form assumed would give rise to a different log amplitude variance expression, eqn. 1.1. Because of the questions raised by this problem, it was decided to measure the turbulence present in our heater section.

B. MEASUREMENTS

1. Equipment

The system used is shown in Figure 20. The Analogic Corporation Data Precision model Data 6000 waveform analyzer sampled the input signal, computed the power spectrum, and then averaged 100 spectra for a final result. The resulting data array could then be passed to the HP-9825B to be recorded on magnetic tape cartridges, scaled, and finally, plotted.

Input signals to the Data 6000 were obtained by modifying components of the C_T^2 system. A single platinum wire temperature probe, with a small constant current applied, generated voltages proportional to the temperature changes in the turbulence. These fluctuations were amplified using the Princeton Applied Research model 113 amplifier available to us, and then fed to the Data 6000. The output array of the Data 6000 was then processed by the HP-9825B to yield dimensionally correct values for plotting of the usual log-log form of the power spectrum.

It was during this phase of our work that the problem mentioned in Chapter 2 with the C_T^2 equipment was discovered. What was thought to be a simple AC bridge used in the turbulence measuring system was found to be a much more complex device. The frequency response of the bridge drastically attenuated the higher frequencies of the turbulence which we were trying to measure. This would effect the inputs provided to the C_T^2 system, so that the values of C_T^2 used previously for normalization of the scintillation strengths must be discounted until the frequency response of the bridge is known.

2. Results

We conducted numerous trials with this spectrum measuring equipment, for various combinations of heaters, fans, and baffle arrangements. Some representative spectra are shown in Figures 21 and 22. The solid line in each case represents the -5/3 slope characteristic of the one dimensional Kolmogorov turbulence function. This particular value

of slope is present only briefly, if at all, in the plots. This leads to the conclusion that we are not in a region of turbulence described by a function of the Kolmogorov form. Since we have not met all the requirements of the Ze'evi theory, we cannot state firmly whether or not it is correct.

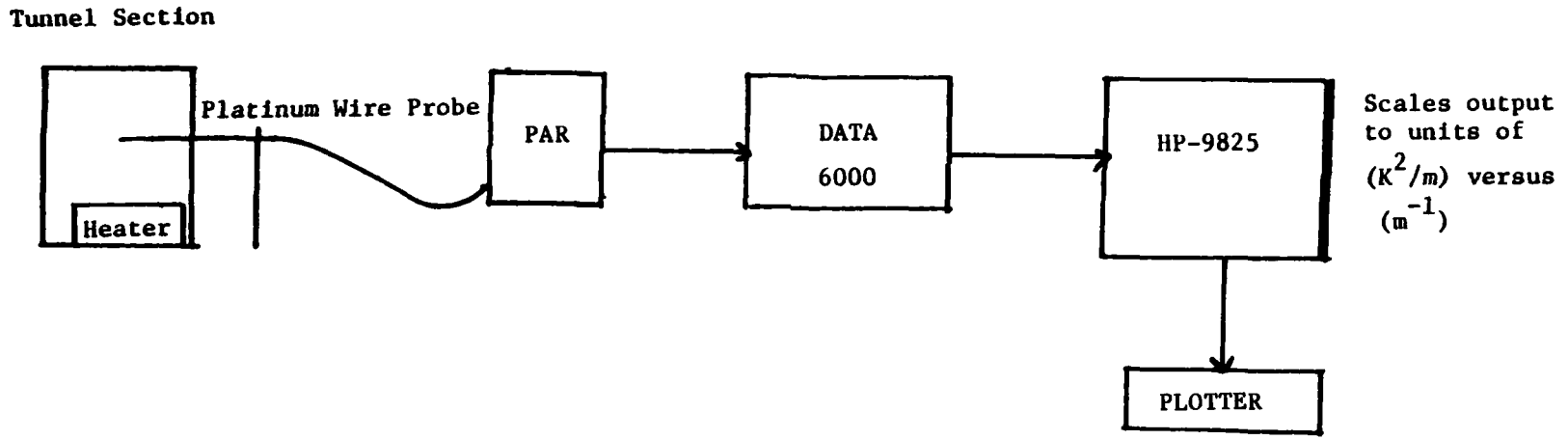

Figure 25. Arrangement for Measuring Power Spectrum.

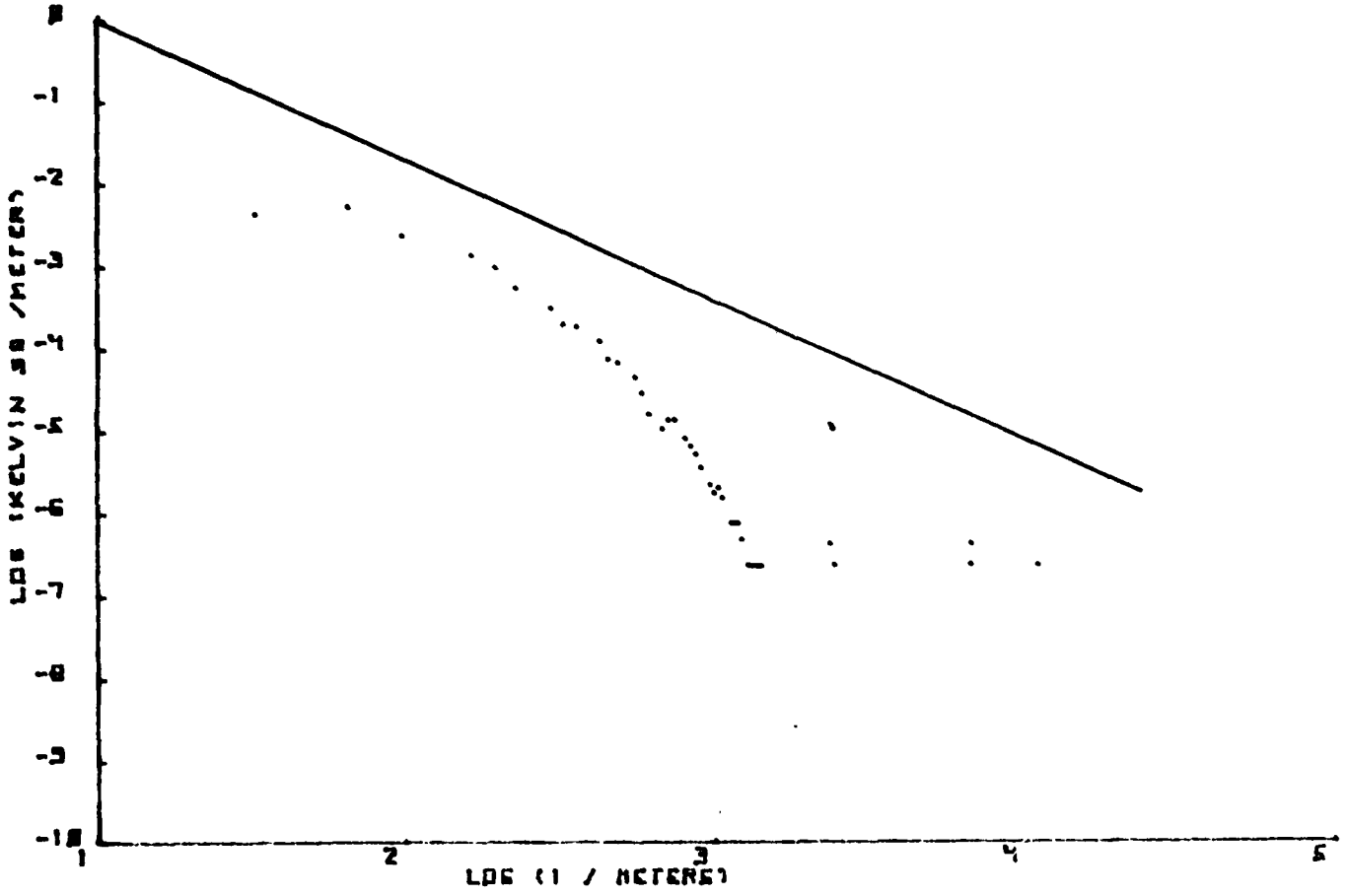

Figure 26. Sample Power Spectrum, Heater and Fan. Solid Line is (-5/3) Slope Characteristic of Kolmogorov Spectrum.

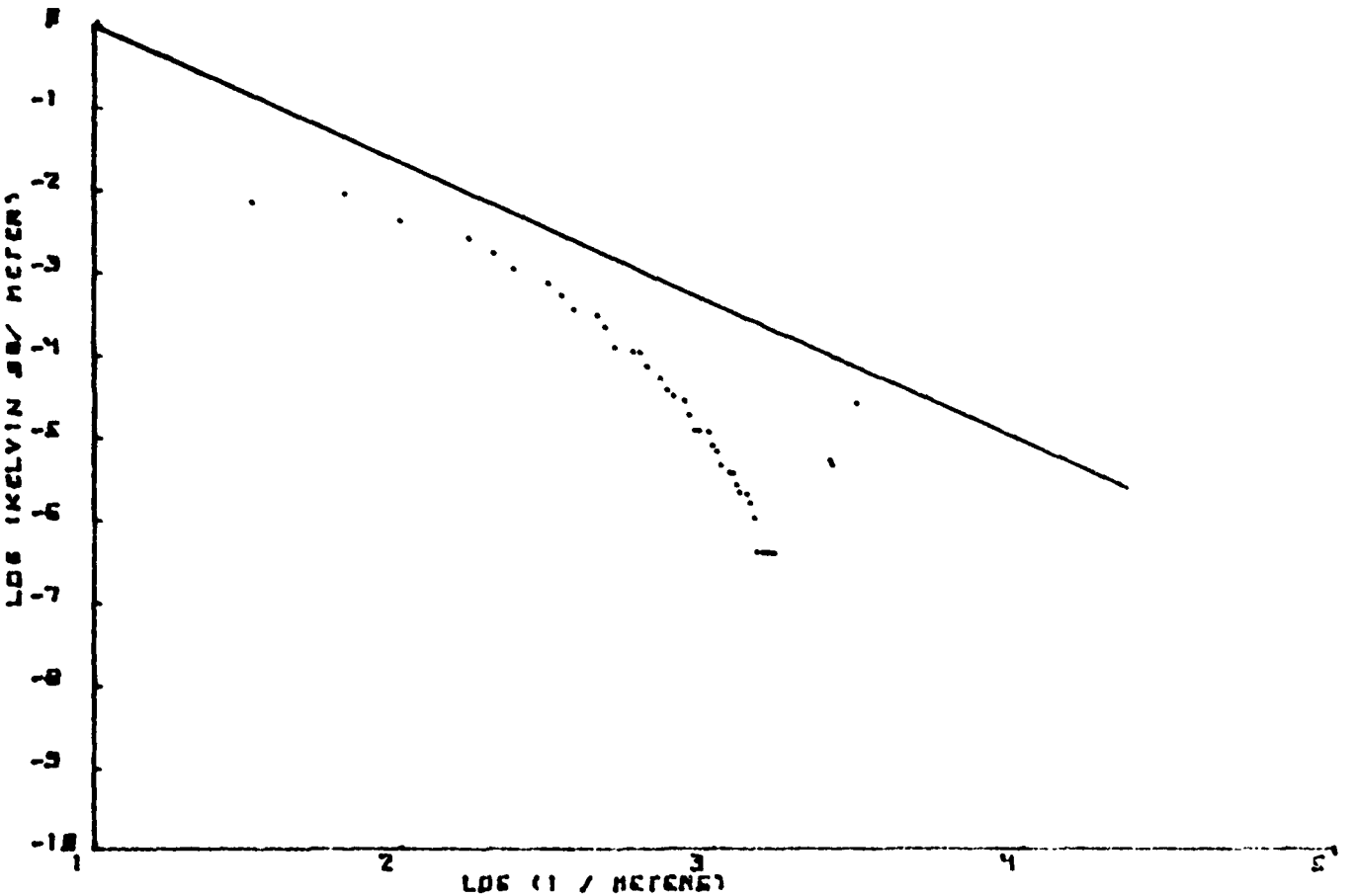

Figure 27. Sample Power Spectrum. Heater Section Solid Line is (-5/3) Slope Characteristic of Kolmogorov Spectrum.

V. CONCLUSIONS

Having reviewed our equipment and presented our results, we make the following statements.

1. We are unable to confirm the Ze'evi path weighting functions for the direct or folded path, although our results tend to follow the general predicted form. We are uncertain whether the discrepancy between experiment and theory is due to some shortcoming in the theory, or the absence of the required Kolmogorov turbulence assumed by Ze'evi.

2. We note that the scintillation of the flat mirror is larger than that of the corner cube, confirming our earlier assumptions.

3. Recommendations. First, the measurements of turbulence begun here should be continued in more detail. Second, the turbulence chamber and heater should be modified in order to provide a source of turbulence consistent with theory.

APPENDIX A

RESULTS OF 12 MAY EXPERIMENT

DIRECT PATH SCINTILLATION DATA - 12 MAY 1983
(CORNER CUBE REFLECTOR)

DISTURBANCE DISTANCE (meters	$\langle \sigma_i \rangle$	$(\langle \sigma_i \rangle^2 \langle \sigma_{quiet} \rangle^2) \times 10^{-2}$
Quiet	.1008 ± .0003	--
1.0	.1026 ± .0008	.0366 ± .0175
5.8	.1176 ± .0026	.3669 ± .0614
10.7	.1237 ± .0026	.5141 ± .0646
15.5	.1626 ± .0038	1.628 ± .1237
20.4	.1829 ± .0070	2.329 ± .2561
25.3	.1987 ± .0148	2.932 ± .5882
30.1	.1650 ± .0122	1.706 ± .4026
35.0	.1701 ± .0053	1.877 ± .1804
39.8	.1961 ± .0110	2.829 ± .4315
44.7	.1928 ± .0049	2.701 ± .1813
49.5	.1776 ± .0055	2.138 ± .1954
54.4	.1878 ± .0089	2.511 ± .3343
60.0	.1260 ± .0205	.5715 ± .5166

FOLDED PATH SCINTILLATION DATA - 12 MAY 1983

CORNER CUBE REFLECTOR

DISTURBANCE DISTANCE (meters)	$\langle \sigma_i \rangle$	$\langle \sigma_i \rangle^2$ $\langle \sigma_{quiet} \rangle^2 \times 10^{-1}$
Quiet Tunnel	.1721 ± .0018	--
1.0	.2468 ± .0036	.3129 ± .0188
5.8	.2720 ± .0042	.4436 ± ± .0237
10.7	.3735 ± .0060	1.0988 ± .0452
15.5	.3757 ± .0106	1.1153 ± .0799
20.4	.4703 ± .0129	1.9156 ± .1215
25.3	.4751 ± .0311	1.9610 ± .2956
30.1	.4989 ± .0261	2.1928 ± .2605
35.0	.5306 ± .0213	2.5190 ± .2261
39.8	.5351 ± .0147	2.5670 ± .1574
44.7	.6628 ± .0124	4.0968 ± .1645
49.5	.6752 ± .0197	4.2628 ± .2661
54.4	.7736 ± .0073	5.6884 ± .1131
60.0	.6338 ± .0595	3.7208 ± .7542

MAY. 12 1983
370,100,10k,0
2121,25.3
Wavelength= 6.33E-07 meters

Scintillation measurements of Sigma
16384 samples for each measurement
Fixed range= 61 meters

# pts	Sigma	Chi Square
1:16373	0.1691	6.13E 02**
1:16350	0.4363	1.42E 03**
2:16382	0.1778	1.17E 03**
2:16374	0.4082	1.04E 03**
3:16356	0.2196	9.25E 02**
3:16293	0.5291	8.72E 02**
4:16341	0.2284	1.44E 03**
4:16239	0.5269	1.21E 03**

Figure 28. Sample Scintillation Statistics.

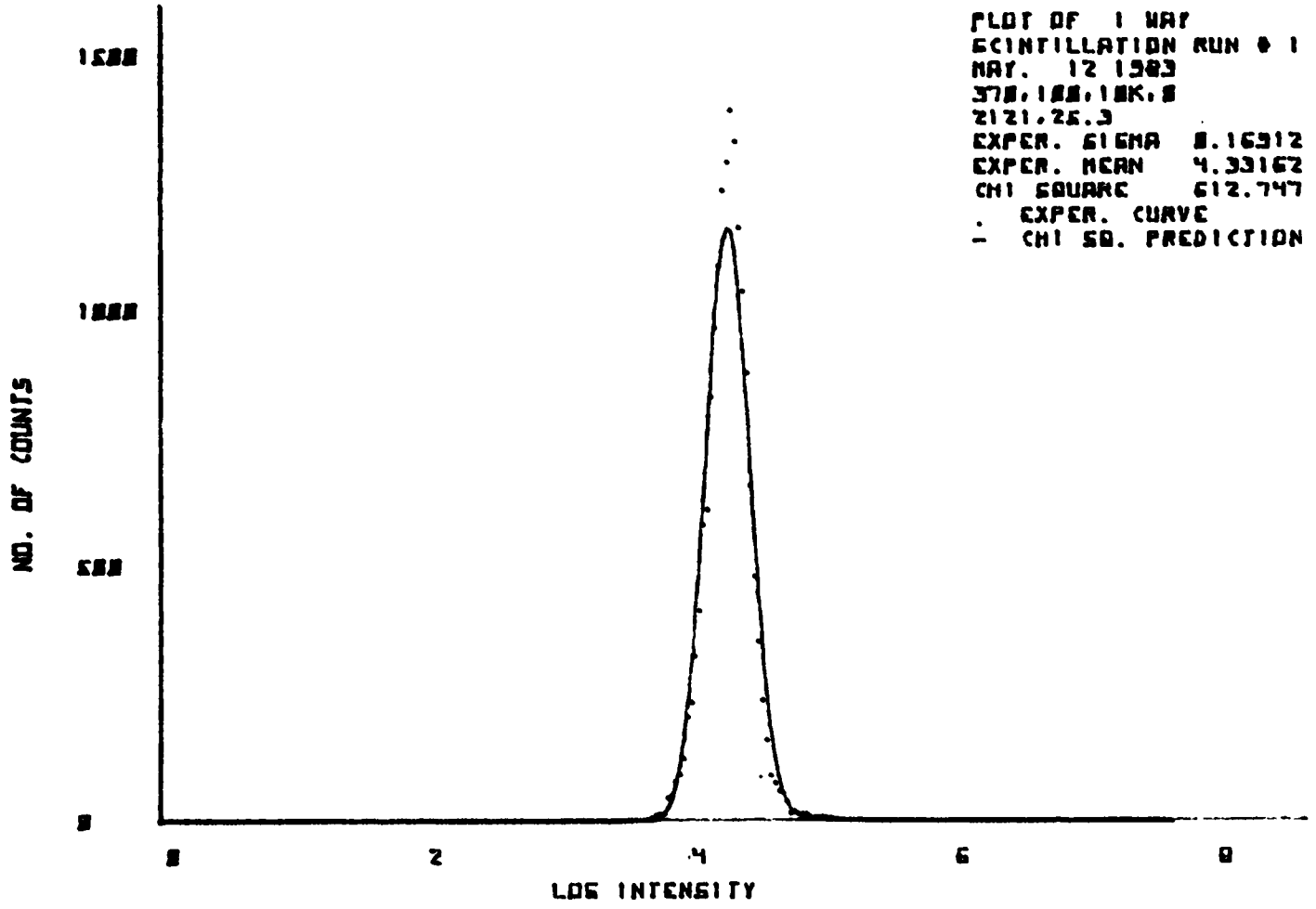

Figure 29. Sample Scintillation Data and Theoretical Curve.

APPENDIX B

RESULTS OF 19 MAY EXPERIMENT

DIRECT PATH SCINTILLATION DATA - 19 MAY 1983
FLAT MIRROR REFLECTOR

DISTURBANCE DISTANCE (meters)	$\langle \sigma_i \rangle$	$(\langle \sigma_i \rangle^2 - \langle \sigma_{quiet} \rangle^2) \times 10^{-2}$
Quiet	.0359 ± .0003	--
25.3	.1430 ± .0025	1.9164 ± .0712
30.1	.1478 ± .0039	2.0560 ± .1153
35.0	.1652 ± .0068	2.6006 ± .2230
39.8	.1451 ± .0034	1.9769 ± .0987
44.7	.1894 ± .0022	3.4587 ± .0834
49.5	.1340 ± .0061	1.6671 ± .1635
54.4	.1750 ± .0132	2.9349 ± .4619
60.0	.0632 ± .0013	.2712 ± .0166

FOLDED PATH SCINTILLATION DATA - 19 MAY 1983
CORNER CUBE

DISTURBANCE DISTANCE (meters)	$\langle \sigma_i \rangle$	$(\langle \sigma_i \rangle^2 - \langle \sigma_{quiet} \rangle^2) \times 10^{-1}$
Quiet	.0603 ± .0041	--
20.4	.2891 ± .0088	.7994 ± .5072
25.3	.3447 ± .0104	1.1518 ± .0718
30.1	.4120 ± .0049	1.6609 ± .0408
35.0	.4066 ± .0162	1.6169 ± .1318
39.8	.4639 ± .0247	2.1160 ± .2292
44.7	.5231 ± .0041	2.7000 ± .0432
49.5	.5196 ± .0117	2.6634 ± .1217
54.4	.6108 ± .0173	3.6944 ± .2114
60.0	.6371 ± .0080	4.0226 ± .1021

FOLDED PATH SCINTILLATION DATA - 19 MAY 1983
FLAT MIRROR

DISTURBANCE DISTANCE (meters	$\langle \sigma_i \rangle$	$(\langle \sigma_i \rangle^2 - \langle \sigma_{quiet} \rangle^2) \times 10^{-1}$
Quiet	.0904 ± .0027	--
25.3	.3127 ± .0138	.8961 ± .0864
30.1	.3486 ± .0058	1.1335 ± .0407
35.0	.3670 ± .0176	1.2652 ± .1293
39.8	.4120 ± .0053	1.6157 ± .0438
44.7	.5574 ± .0151	3.0252 ± .1684
49.5	.6144 ± .0360	3.6932 ± .4424
54.4	.8596 ± .0185	7.3074 ± .3181
60.0	.7580 ± .0113	5.6639 ± .1714

DIRECT PATH SCINTILLATION DATA - 19 MAY 1983
CORNER CUBE

DISTURBANCE DISTANCE (meters)	$\langle \sigma_i \rangle$	$(\langle \sigma_i \rangle^2 - \langle \sigma_{quiet} \rangle^2) \times 10^{-2}$
Quiet	.0384 ± .0005	--
20.4	.1327 ± .0069	1.6135 ± .1842
25.3	.1818 ± .0058	3.1576 ± .2120
30.1	.1632 ± .0033	2.5160 ± .1086
35.0	.1861 ± .0085	3.3159 ± .3160
39.8	.1842 ± .0103	3.2455 ± .3795
44.7	.2266 ± .0063	4.9873 ± .2855
49.5	.1622 ± .0019	2.4834 ± .0618
54.4	.1412 ± .0049	1.8463 ± .1384
60.0	.0854 ± .0006	.5810 ± .0114

APPENDIX C

RESULTS OF 9 SEPTEMBER EXPERIMENT

FOLDED PATH SCINTILLATION DATA - 9 SEPT 1983
FLAT MIRROR

DISTURBANCE DISTANCE (meters)	$\langle \sigma_i \rangle$	$(\langle \sigma_i \rangle^2 - \langle \sigma_{quiet} \rangle^2) \times 10^{-1}$
Quiet	.0557 ± .0008	--
12.0	.1622 ± .0060	.2320 ± .0019
24.0	.2753 ± .0092	.7270 ± .0051
36.0	.3628 ± .0027	1.2850 ± .0020
45.6	.4902 ± .0080	2.3720 ± .0078
50.4	.3852 ± .0268	1.4530 ± .0206
52.8	.4792 ± .0066	2.2650 ± .0063
55.2	.3615 ± .0114	1.2760 ± .0082
57.6	.3998 ± .0227	1.5680 ± .0182
60.0	.3999 ± .0139	1.5690 ± .0111

DIRECT PATH SCINTILLATION DATA - 9 SEPT 1983
FLAT MIRROR

DISTURBANCE DISTANCE (meters)	$\langle \sigma_i \rangle$	$(\langle \sigma_i \rangle^2 - \langle \sigma_{quiet} \rangle^2) \times 10^{-2}$
Quiet	.0278 ± .0002	--
12.0	.0956 ± .0030	.8374 ± .0574
24.0	.1352 ± .0076	1.7510 ± .2055
36.0	.1502 ± .0006	2.1801 ± .0181
45.6	.1241 ± .0030	1.4620 ± .0745
50.4	.0833 ± .0020	.6261 ± .0333
52.8	.0806 ± .0031	.5714 ± .4998
55.2	.0852 ± .0029	.6476 ± .0494
57.6	.0737 ± .0021	.4661 ± .0310
60.0	.0742 ± .0008	.4728 ± .0119

FOLDED PATH SCINTILLATION DATA - 9 SEPT 1983
CORNER CUBE

DISTURBANCE DISTANCE (meters)	$\langle \sigma_i \rangle$	$(\langle \sigma_i \rangle^2 - \langle \sigma_{quiet} \rangle^2) \times 10^{-1}$
Quiet	.0512 ± .0030	--
12.0	.1819 ± .0038	.3047 ± .0140
24.0	.3006 ± .0076	.8773 ± .0460
36.0	.4346 ± .0284	1.8626 ± .2470
45.6	.4698 ± .0341	2.180 ± .3200
50.4	.4640 ± .0149	2.1270 ± .1380
52.8	.4785 ± .0058	2.2630 ± .0560
55.2	.5148 ± .0132	2.6245 ± .1360
57.6	.5324 ± .0238	2.8080 ± .2530
60.0	.5552 ± .0305	3.0570 ± .3390

DIRECT PATH SCINTILLATION DATA - 9 SEPT 1983
CORNER CUBE

DISTURBANCE DISTANCE (meters)	$\langle \sigma_i \rangle$	$(\langle \sigma_i \rangle^2 - \langle \sigma_{quiet} \rangle^2) \times 10^{-2}$
Quiet	.0252 ± .0006	--
12.0	.0983 ± .0038	.9025 ± .0748
24.0	.1302 ± .0040	1.6330 ± .1042
36.0	.1402 ± .0088	1.9024 ± .2468
45.6	.1165 ± .0068	1.2940 ± .1585
50.4	.0819 ± .0051	.6075 ± .0836
52.8	.0769 ± .0035	.5277 ± .0539
55.2	.0827 ± .0013	.6203 ± .0217
57.6	.0786 ± .0011	.5549 ± .0176
60.0	.0771 ± .0010	.5312 ± .0157

APPENDIX D

RESULTS OF 15 OCTOBER EXPERIMENT

FOLDED PATH SCINTILLATION DATA - 15 OCT 1983
CORNER CUBE

DISTURBANCE DISTANCE (meters)	$\langle \sigma_i \rangle$	$(\langle \sigma_i \rangle^2 - \langle \sigma_{quiet} \rangle^2) \times 10^{-1}$
Quiet	.0225 ± .0010	--
7.2	.1456 ± .0075	.2069 ± .0218
14.4	.1932 ± .0064	.3682 ± .0247
21.6	.2806 ± .0112	.7823 ± .0628
28.8	.3504 ± .0188	1.2228 ± .1318
36.0	.4017 ± .0232	1.6080 ± .1864
43.2	.2621 ± .0150	.6819 ± .0786
48.0	.3540 ± .0103	1.2480 ± .0729
52.8	.3976 ± .0327	1.5760 ± .2600
57.6	.5233 ± .0147	2.7330 ± .1538
60.0	.5408 ± .0269	2.9190 ± .2910

DIRECT PATH SCINTILLATION DATA - 15 OCT 1983
CORNER CUBE

DISTURBANCE DISTANCE (meters)	$\langle \sigma_i \rangle$	$(\langle \sigma_i \rangle^2 \quad \langle \sigma_{quiet} \rangle^2) \times 10^{-2}$
Quiet	.0205 ± .0007	--
7.2	.0814 ± .0036	.6206 ± .0587
14.4	.1064 ± .0075	1.0890 ± .1596
21.6	.1293 ± .0081	1.6228 ± .2095
28.8	.1415 ± .0098	1.9600 ± .2774
36.0	.1507 ± .0098	2.2290 ± .0030
43.2	.0738 ± .0024	.5026 ± .0355
48.0	.0770 ± .0017	.5509 ± .0263
52.8	.0500 ± .0042	.2080 ± .0421
57.6	.0548 ± .0016	.2583 ± .0178
60.0	.0566 ± .0012	.2783 ± .0139

APPENDIX E

RESULTS OF 11 NOVEMBER EXPERIMENT

DIRECT PATH SCINTILLATION DATA - 11 NOV 1983
CORNER CUBE

DISTURBANCE DISTANCE (meters)	$\langle \sigma_i \rangle$	$(\langle \sigma_i \rangle^2 - \langle \sigma_{quiet} \rangle^2) \times 10^{-2}$
Quiet	.0302 ± .0008	--
1.0	.0333 ± .0008	.0197 ± .0072
4.8	.0531 ± .0017	.1908 ± .0187
12.0	.1011 ± .0034	.9309 ± .0689
19.2	.1240 ± .0101	1.4460 ± .2505
26.4	.1220 ± .0127	1.4000 ± .3099
33.6	.1663 ± .0071	2.6740 ± .2362
40.8	.1397 ± .0152	1.8600 ± .4247
48.0	.1326 ± .0038	1.6670 ± .1009
55.2	.0979 ± .0031	.8672 ± .0609
60.0	.0692 ± .0017	.3877 ± .0240

FOLDED PATH SCINTILLATION DATA - 11 NOV 1983
CORNER CUBE

DISTURBANCE DISTANCE (meters)	$\langle \sigma_i \rangle$	$(\langle \sigma_i \rangle^2 - \langle \sigma_{quiet} \rangle^2) \times 10^{-1}$
Quiet	.0349 ± .0026	--
1.0	.0456 ± .0023	.0086 ± .0028
4.8	.0736 ± .0024	.0420 ± .0040
12.0	.1526 ± .0018	.2207 ± .0058
19.2	.2015 ± .0135	.3938 ± .0544
26.4	.2005 ± .0208	.3898 ± .0834
33.6	.3836 ± .0256	1.4620 ± .1964
40.8	.3770 ± .0424	1.4090 ± .3197
48.0	.5020 ± .0180	2.5080 ± .1807
55.2	.5690 ± .0363	3.2250 ± .4131
60.0	.5562 ± .0295	3.0810 ± .3282

LIST OF REFERENCES

1. Tatarski, V.I., The Effects of the Turbulent Atmosphere on Wave Propagation, Keter Press Binding, Israel, 1971.

2. Speer, B.A., and Parker, F.H., Measurements of Direct Path and Folded Path Optical Scintillation, Master's Thesis, Naval Postgraduate School, December 1982.

3. Costantine, A.G., Measurements of Direct Path and Folded Path Optical Scintillation Path Weightings, Master's Thesis, Naval Postgraduate School, June 1983.

4. Ze'evi, A., Optical Scintillation Along Folded Paths, Ph.D thesis, Naval Postgraduate School, March 1982.

5. Flenniken, R.J., Weighting for the Modulation Transfer Function, Master's Thesis, Naval Postgraduate School, June 1983.

INITIAL DISTRIBUTION LIST

		No. Copies
1.	Defense Technical Information Center Cameron Station Alexandria, Virginia 22314	2
2.	Library, Code 0142 Naval Postgraduate School Monterey, California 93943	2
3.	G. E. Schacher, Chairman, Code 61Sq Department of Physics Naval Postgraduate School Monterey, California 93943	2
4.	E. C. Crittenden, Jr., Code 61Ct Department of Physics Naval Postgraduate School Monterey, California 93943	2
5.	Professor E. A. Milne, Code 61Mn Department of Physics Naval Postgraduate School Monterey, California 93943	4
6.	M. C. Drong, Code 1230 Pacific Missile Test Center Point Mugu, NAS, California 93042	1
7.	A. G. Costantine Department of Physics USMA West Point, NY 10996	1
8.	L.M. Henry 15 Greenway, 6-D Houston, TX 77069	1
9.	Captain James Baumann, Code 1230.2 Pacific Missile Range Point Mugu, NAS, California 93042	1

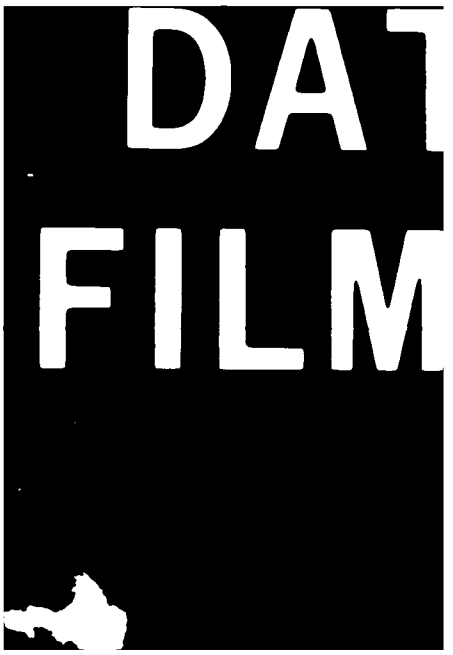
DAT
FILM